6.1 INTRODUCTION

Quality by Design (QbD) is defined as "a systematic approach that begins with predefined objectives and emphasizes product and process understanding and process control, based on quality risk management to pharmaceutical development". It relates developing formulations and manufacturing processes to confirm a predefined quality. Thus, QbD needs an understanding how formulation and process variables impact product quality (1).

ICH defined CQA as "a CQA is a quality attribute (a physical, chemical, biological or microbiological property or characteristic) that must be controlled (directly or indirectly) to ensure the product meets its intended safety, efficacy, stability and performance". Risk assessment methods mentioned in ICH guideline Q9 are Failure Mode Effects Analysis (FMEA), Failure Mode, Effects and Criticality Analysis (FMECA) etc. These principles help to identify Critical Process Parameters (CPPs) that can affect the quality of final product. The relationship between the input variables (formulation and process parameters) and the critical quality attributes can be described in the design space (2,3).

Thus, QbD helps in understanding the effect of critical processing parameters (CPPs) by identifying risk identification (Ishikawa diagram), risk analysis (Screening design) and optimization using Design of Experiment (Factorial design, Box Behnken Design, Central Composite Design, etc.) on Critical Quality Attributes (CQA) of final product (4).

Response surface methodology (RSM) is the group of mathematical and statistical techniques which is used to elucidate functional relationship between a response of interest (dependent variables) and a number of input variables (independent variables). Box Behnken Design (BBD) devised by George Box and Donald Behnken in 1960, a type of RSM widely used for optimization purpose. It is a tool for multivariate optimization characterized by set of points lying at the midpoint of each edge of a multi dimensional cube and center point replicates. It do not include axial points and they ensures that all factors are never simultaneously set at their highest and lowest levels. It is particularly useful when extreme treatment combinations need to be avoided (5). The regression equation for the response is calculated using the equation 6.1:

$$Y = b_o + b_1X_1 + b_2X_2 + b_3X_{3+}b_{11}X_1^2 + b_{22}X_2^2 + b_{33}X_3^2 + b_{12}X_1X_2 + b_{13}X_1X_3 + b_{23}X_2X_3 \ldots\ldots\ldots Equation\ 6.1$$

In this mathematical equation, X_1, X_2 and X_3 represents independent variables. b_0 is a constant and b_1, b_2 & b_3 are linear coefficients. However, b_{12}, b_{13} & b_{23} are interaction coefficients and b_{11}, b_{22} & b_{33} represent the quadratic coefficients which are computed from the predicted responses.

Lurasidone hydrochloride (LH) is an atypical antipsychotropic agent for the treatment of schizophrenia and bipolar disorder. Clinical evidences showed that LH had a more significant efficacy in treating the psychopaths with cognitive impairment than other commercial available antipsychotics. As a BCS class II drug, LH has poor bioavailability with absolute oral bioavailability of 9-19% in human and ~23% in rats. In addition to extensive first-pass metabolism (only 1% of unchanged lurasidone was recovered in urinary and biliary routes after intravenous administration of LH), incomplete absorption of LH due to poor water solubility and low dissolution is the major reason for its low oral bioavailability (6).

Hence, LH loaded solid lipid nanoparticles (LH-SLNs) were prepared and optimized by applying QbD concept using two statistical approaches: Plackett Burman Design (Screening design) and Box Behnken Design, a type of RSM.

6.2 MATERIALS

Lurasidone HCl was received as a gift sample from Alembic Pharmaceuticals Ltd., Vadodara, India. Glyceryl Monostearate was purchased from Loba Chemie Pvt Ltd., Mumbai, India. Poloxamer 188 and Sodium deoxycholate was purchased from Sigma Aldrich, Germany. All other chemicals and reagents used were of analytical grade.

6.3 EQUIPMENT

Name of Equipment	Manufacturer
High speed homogenizer (HSH)	T-25 digital Ultra-Turrax, IKA® India Private Limited, India
High Pressure Homogenizer (HPH)	PandaPLUS, GEA Niro Soavi, Italy
Zeta sizer	Zeta sizer Nano series, Malvern Instruments, UK
Centrifuge CPR 30	Remi, India
VirTis Advantage Plus XL-70	SP Scientific, USA
Transmission Electron Microscope (TEM)	Philips, Tecnai 20, Holland
UV-VIS Spectrophotometer	UV 1800, Shimadzu AS, Japan
Differential Scanning Calorimeter (DSC)	Shimadzu, Japan
Fourier Transform Infra-red spectrophotometer (FTIR)	Shimadzu, Japan

6.4 SCREENING OF SOLID LIPID

Screening of solid lipid was performed as described in section 4.4 and amount of dissolved drug was determined by measuring absorbance using UV- spectroscopy (UV 1800, Shimadzu AS, Japan) at 318 nm.

6.5 PREPARATION OF SOLID LIPID NANOPARTICLES

Solid lipid nanoparticles were prepared using High Pressure Homogenizer (HPH). In this method, solid lipid was melted 5 °C above the melting point of lipid; LH was dissolved in lipid and then added to a mixture of surfactants and water, previously heated at the same temperature. A pre-emulsion was obtained under stirring with the high speed homogenizer. This pre-emulsion was further passed through high pressure homogenizer. The o/w nanoemulsion formed was immediately cooled down to room temperature to generate SLN (7,8). The resultant LH loaded SLN dispersion was subjected to characterization.

6.6 EXPERIMENTAL DESIGN

6.6.1 Initial Risk Assessment: Ishikawa diagram

Several Ishikawa diagrams (also known as the fish-bone diagram, or cause-and-effect diagram) were constructed to identify the potential risks and corresponding causes. Specifically, two major quality attributes, particle size (PS) and drug entrapment efficiency (EE), were defined and further delineated to identify all potential risks (9).

6.6.2 Preliminary investigation of critical variables

Key variables were identified from risk analysis and its preliminary optimization was carried out by changing one variable at a time while keeping the other constant. The effects of selected variables on the particle size and entrapment efficiency were evaluated to determine the optimal lower and upper values for a screening design study.

6.6.3 Risk Analysis: Plackett Burman Design (PBD)

The screening of various process and formulation variables was carried out using PBD and their relative influence on the particle size and entrapment efficiency of the LH loaded SLNs. The selection of the low and high values was based on the preliminary study results. The PBD was constructed with 12 runs using Minitab version 16 (Minitab Inc., State College, PA,USA).

Key factors were X_1: Homogenization speed, X_2: Homogenization time, X_3: Homogenization pressure, X_4: Homogenization cycle, X_5: Concentration of lipid, X_6: Concentration of surfactant, and X_7: Concentration of sodium deoxycholate. Particle size (Y_1) and entrapment efficiency (Y_2) were taken as response variables. Main effect plot, Pareto chart, Normal plot and half normal plot was constructed using Minitab software (ver. 16.2.1., Minitab Inc.,USA).

6.6.4 Optimization using Box Behnken Design (BBD): A response surface methodology

A three-factor, three-level Box–Behnken statistical design was applied to study the impact of variables on measured responses (dependent variables). The lipid concentration, homogenization pressure and homogenization cycle were used as three independent variables. Particle size (Y_1) and entrapment efficiency (Y_2) were used as three dependent variables in the present study. The coded and actual value of independent variables are shown in table 6.1.

Table 6.1: The coded and actual values of independent variables of LH-SLNs

Factors	Levels		
	-1	**0**	**+1**
X_1: Lipid Concentration (%)	7.5	10	12.5
X_2: Homogenization Pressure (bar)	600	800	1000
X_3: Homogenization cycle	7	9	11

All statistical treatments of design were performed using Design Expert software (ver. 8.0.7.1, Stat- Ease Inc., USA). Response surface plots and contour plots were generated using design expert software. Check point batch suggested by software was prepared and the percentage relative error of each response was calculated using following equation in order to judge validity of the model.

$$\%\ Relative\ Error = \frac{Predicted\ value - Experimental\ value}{Predicted\ value} * 100$$

6.6.5 Optimization using Desirability function

For simultaneous optimization of response variables (PS and EE), desirability function (multi-response optimization technique) was applied and total desirability was calculated using Design Expert software (version 7.0.3, Suite, Minneapolis, MN). The desirability lies between 0 and 1 and it represents the closeness of a response to its ideal value (8).

6.6.6 Analysis of design space robustness

Overlay plot was generated using design expert to evaluate robustness of established design space with selecting response to higher and lower value of established design space. The software suggested values for independent variables in and around established design space along with value of the desired responses (10).

6.6.7 Statistical Analysis

The results were presented as mean ± standard error of the mean. The results were analyzed using the statistical software Minitab 16 and Design expert 7. The experimental data were validated by ANOVA, regression coefficient, and p value less than 0.05 was considered as significant.

6.7 LYOPHILIZATION OF SLNs AND OPTIMIZATION OF CRYOPROTECTANT

The optimized SLN formulation was lyophilized using lyophilizer (Virtis, SP Scientific, USA). Different cryoprotectants (Trehalose dihydrate, Mannitol and Sucrose) at different ratio (1:1 %w/w, 1:2 %w/w, 1:3 %w/w) were tried to select the appropriate cryoprotectant. SLN dispersion (2 ml) was taken in 10 ml semi-stoppered vials with rubber closures and frozen for 24 h at -80°C and then lyophilized for 24 h in the lyophilizer (Virtis, SP Scientific, USA). Finally, the lyophilized samples were sealed under anhydrous conditions and stored until further characterization (11,12). Ratio of final particle size (after lyophilization, S_f) and initial particle size (before lyophilization, S_i) was calculated to finalize the suitable cryoprotectant based on lowest S_f/S_i ratio.

6.8 CHARACTERIZATION

6.8.1 Determination of particle size

Particle size was determined as per procedure described in section 4.8.1.

6.8.2 Zeta potential measurement

Zeta potential was determined as per procedure described in section 4.8.2.

6.8.3 Determination of entrapment efficiency

The percentage entrapment efficiency was determined by measuring amount of unentrapped drug in SLN dispersion. SLN dispersion was centrifuged at 12000 rpm for 30 min so as to settle the SLN pellet. 1 ml of supernatant was dissolved in 10 ml of methanol, the solution was filtered and amount of free drug in the supernatant was determined by measuring absorbance at 230 nm in UV spectrophotometer (UV 1800, Shimadzu AS, Japan). % EE was calculated from the following equation:

$$\%EE = \frac{\text{Total amount of drug added} - \text{free drug}}{\text{Total amount of drug added}} \times 100 \ldots\ldots\ldots\ldots\ldots\ldots\ldots\ldots \text{(Equation 6.2)}$$

6.8.4 Determination of total drug content

1 ml of LH-SLNs dispersion was dissolved in methanol. Suitable dilution was made and absorbance was measured at 230 nm using UV spectrophotometer to determine amount of LH present.

6.8.5 Fourier Transform Infra-red spectroscopy (FTIR)

The IR spectra of LH, GMS, physical mixture of LH and GMS and lyophilized LH-SLNs were recorded on Fourier Transform Infra-red spectrophotometer (Shimadzu, Japan).

6.8.6 Differential Scanning Colorimeter (DSC)

The DSC thermograms of LH, GMS, physical mixture of LH and GMS and lyophilized LH-SLNs were taken on a Differential Scanning Calorimeter (Shimadzu DSC-60) between 40 and 250 °C at a heating rate of 10 °C/min with Nitrogen supplied at 30 ml/min.

6.8.7 X Ray Diffraction (XRD) study

The X-ray diffraction (XRD) studies of pure LH, GMS, physical mixture of LH and GMS and lyophilized LH-SLNs were carried out by wide angle X-Ray scattering (Philips, PW 1710) with a copper anode using Sc as detector.

6.8.8 Transmission Electron Microscopy (TEM)

For this study, 20 µl of sample was taken on carbon filmcoated on copper grid and allowed to air dry. Then it was treated with phosphotungstic acid for negative staining. After 5min the grid was placed in the sample probe inserted in Transmission Electron Microscope (Philips, Tecnai 20, Holland) and observed at 200 kV accelerating voltage.

6.9 IN VITRO DRUG RELEASE STUDY

In vitro drug release of LH-SLNs was carried out same as procedure described in section 4.9 except LH-loaded SLN dispersion and LH suspension equivalent to 20 mg of LH was placed in the dialysis bag and phosphate buffer pH 6.8 containing 0.1% SLS. Drug concentration was determined using UV spectroscopy at 232 nm.

6.10 EX VIVO PERMEATION STUDY

Ex vivo permeation study of LH-SLNs was carried out same as procedure described in section 4.10 except LH-loaded SLN dispersion and LH suspension equivalent to 20 mg of LH was taken for the study and phosphate buffer pH 7.4 containing 0.1% SLS. Drug concentration was determined using UV spectroscopy at 232 nm.

6.11 STABILITY STUDY

Stability study of LH loaded SLN was carried out as per procedure described in section 4.11

6.12 RESULTS AND DISCUSSION

6.12.1 Screening of solid lipid

The maximum solubility of LH was obtained in Glyceryl monostearate (GMS) (Figure 6.1). Therefore, GMS was chosen as solid lipid for development of SLNs owing to its high potential for solubilization of drug.

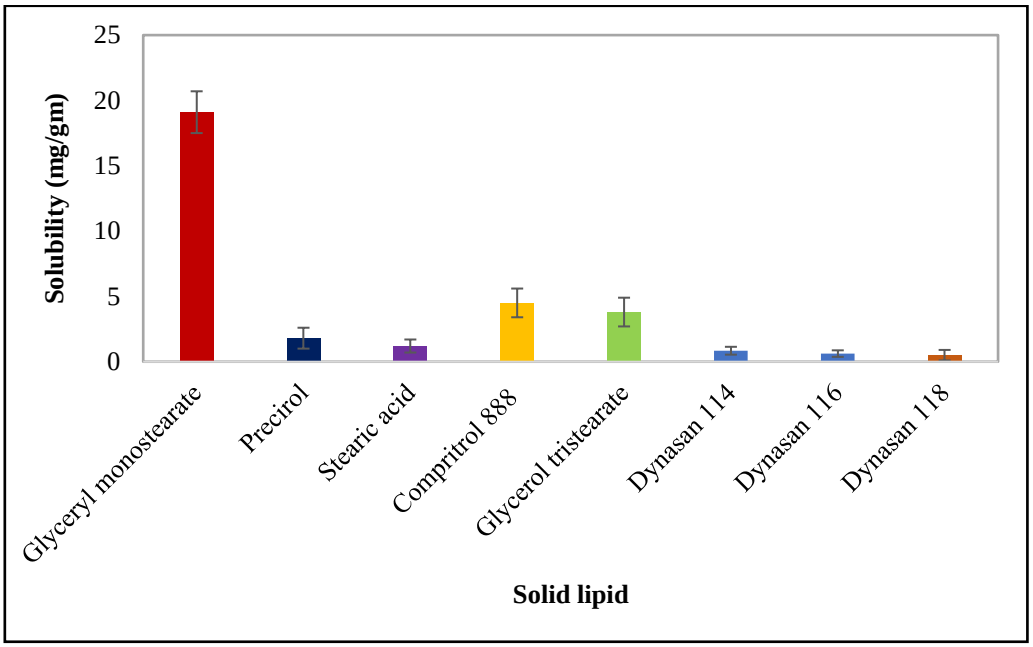

Figure 6.1: Solubility of Lurasidone HCl in various lipids

6.12.2 Risk identification: Ishikawa diagram

SLNs particle size and drug entrapment efficiency are two very critical product qualities, and an understanding and awareness of the potential risks is very important. To accomplish this, two cause-and-effect diagrams (Ishikawa diagram) were constructed to identify the potential causes of product variability (Figure 6.2 & 6.3).

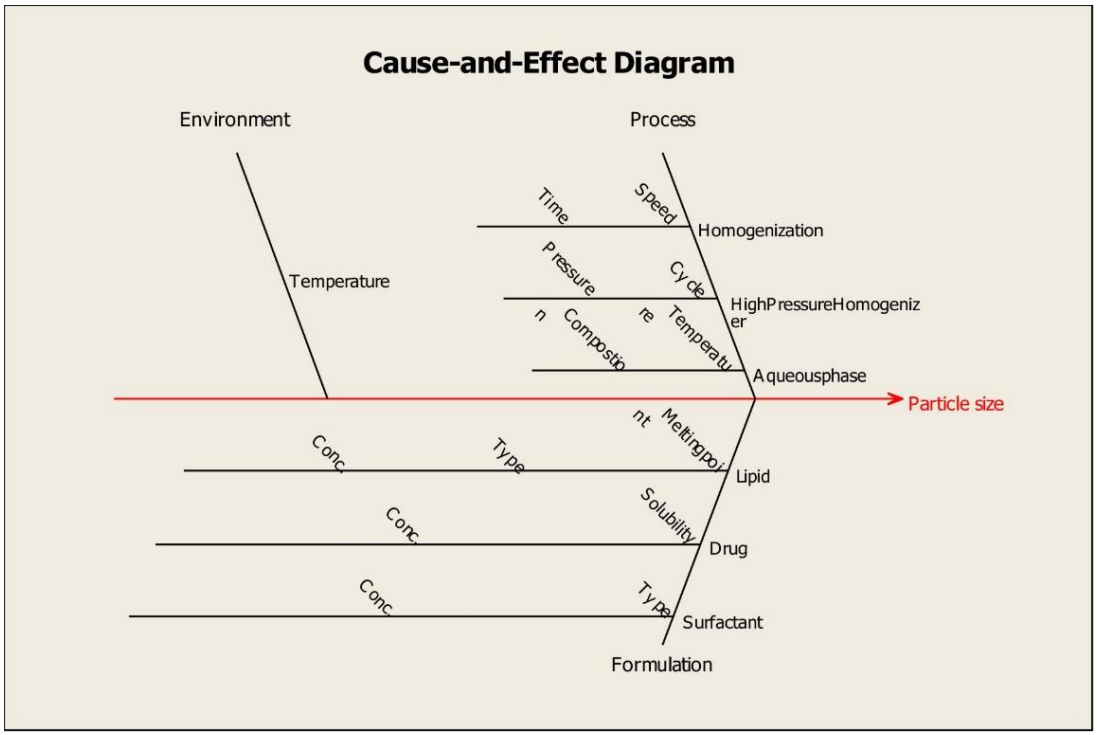

Figure 6.2: Ishikawa diagram illustrating factors that may have impact on the particle size of LH-SLNs

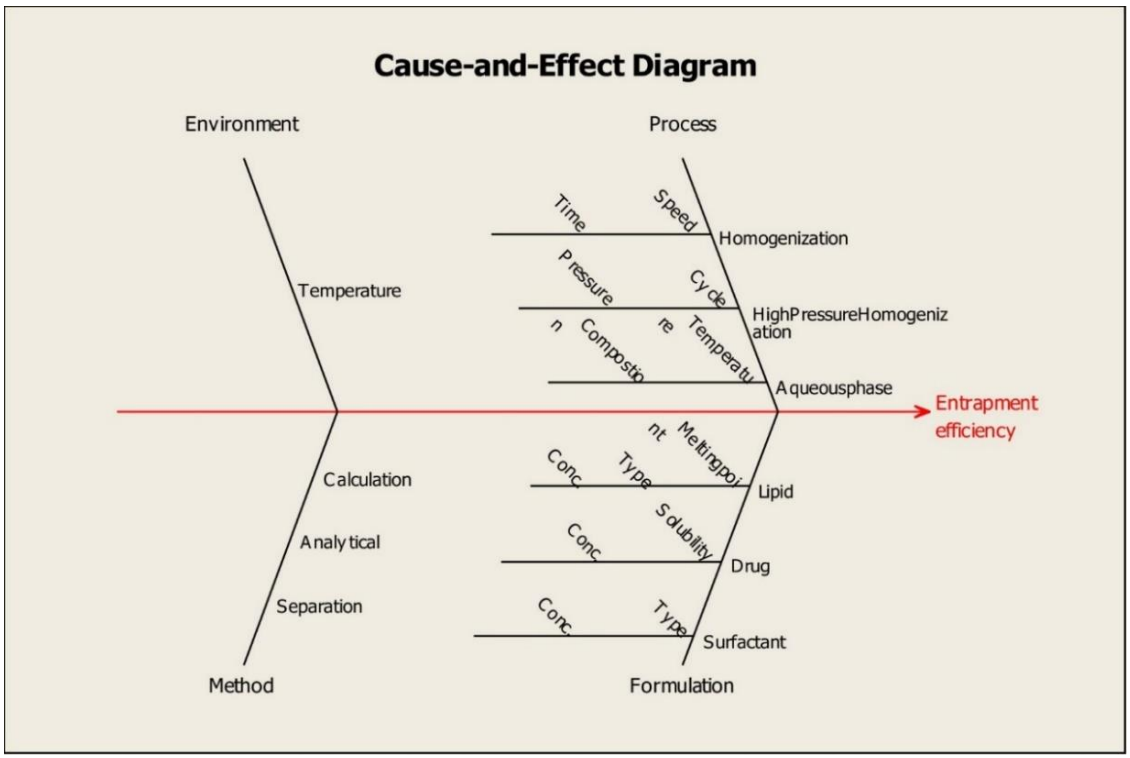

Figure 6.3: Ishikawa diagram illustrating factors that may have impact on the entrapment efficiency of LH-SLNs

6.12.3 Preliminary investigation of variables

6.12.3.1 Influence of process variables

6.12.3.1.1 Influence of homogenization speed

It was observed that homogenization speed had major effect on particle size as compared to entrapment efficiency (Table 6.2). As the homogenization speed was increased from 8000 to 12000 rpm, gradual increase in particle size was observed. This might be because at higher homogenization speed, higher shear rate was generated led to increase in viscosity of continuous phase. Viscosity of lipid phase plays an important role for formulation characteristics in the high speed homogenization. Shearing mechanisms predominate when viscosities increase, leading to larger particle sizes and wider distributions (8). Precipitation of lipid phase occurred at 14000 rpm because of higher viscosity of lipid phase. In case of EE, it was observed that EE was not significantly affected with homogenization speed.

Table 6.2: Effect of homogenization speed on particle size and entrapment efficiency of LH-SLNs

Homogenization Speed (rpm)	Particle size (nm)	Entrapment efficiency (%)
8000	110.2±3.1	72.34±3.58
10000	189.7±4.7	70.31±4.40
12000	247.9±5.8	71.20±2.06
14000	Precipitation	-

6.12.3.1.2 Influence of homogenization time

It was observed that homogenization time had similar effect as that of homogenization speed. As homogenization time increased from 1 min to 5 min, PS was also increased from 147.2 nm to 308.4 nm (Table 6.3). This might be attributed to longer duration of homogenization lead to higher shear rate which increased viscosity and ultimately increased PS. EE was not significantly affected by changing homogenization time.

Table 6.3: Effect of homogenization time on particle size and entrapment efficiency of LH-SLNs

Homogenization time (min)	Particle size (nm)	Entrapment efficiency (%)
1	147.2±5.7	69.00±2.20
2	223.3±3.5	71.16±3.10
5	308.4±8.2	70.15±2.10

6.12.3.1.3 Influence of homogenization pressure

High Pressure Homogenizer (HPH) has a pump that pulls the coarse emulsion into a chamber on its backstroke and then forces it through a narrow valve at the end of the chamber on its forward stroke. As the coarse emulsion passes through the valve it experiences a combination of intense disruptive forces (turbulence, shear and cavitation) that cause the larger droplets to be broken down into smaller ones (10).

In a high-pressure homogenizer, the oil and water mixture is subjected to intense turbulent and shear flow fields. Turbulence is said to be the predominant mechanism, even through laminar shear and cavitation may also play an important role. Turbulence leads to the break up of the dispersed phase into small droplets (13). Considering these mechanisms, particles deformation is proportional to the system energy which is directly related to the pressure. Later, both turbulence and viscous shearing mechanisms were considered to happen simultaneously, depending on the system composition, its energy and thus pressure (8).

It was observed that applied pressure was high influencing parameter on both, PS and EE (Table 6.4). As the applied pressure was increased from 200 to 800 bar, PS was gradually decreased from 355 nm to 103 nm (Table 6.4). This could be attributed to inertial forces dominate the process at high pressure and droplets break up due to pressure fluctuations from turbulence (8) which led to decrease in PS. The droplet size tends to decrease when the homogenization pressure or number of passes increases because the interfacial tension decreases, the emulsifier adsorption rate increases, and the disperse-to-continuous phase viscosity ratio falls within a certain range (10). However, further increase in pressure from 800 bar to 1000 bar, led to increase in PS. This could be due to the increased kinetic energy of the system, resulting in increased particle collision and, thereby coagulation. The high rate of particle collisions also distorts the surfactant film coating the particle surface and enhances particle

aggregation (14). It was observed that EE was unchanged till 600 bar of applied pressure. Increasing pressure form 600 to 800 bar reduced EE. This could be due to reduction of particle size led to loss of drug which reduced EE. Further increase in pressure from 800 to 1000 bar led to aggregation of particles which increased EE.

Table 6.4: Effect of homogenization pressure on particle size and entrapment efficiency of LH-SLNs

Homogenization pressure (bar)	Particle size (nm)	Entrapment efficiency (%)
200	355.4±4.9	76.10±2.20
400	211.1±3.5	78.60±3.42
600	136.4±3.1	77.34±2.36
800	103.2±1.9	68.13±2.05
1000	277.4±2.8	71.20±3.40

6.12.3.1.4 Influence of homogenization cycle

Here, Homogenization cycle is the number of passes applied. It was observed that as the no. of passes increased, PS was decreased significantly upto 7 cycles. However, further increase in homogenization cycle from 9 to 11 resulted in increased PS (Table 6.5). This might be due to the high kinetic energy of small particles which led to aggregation of particles. It was observed that EE was not significantly influenced by homogenization cycle. After 5 cycles EE was decreased because of loss of drug as PS was decreased. However, further increase in number of cycles from 7 to 11, decreased EE due to aggregation of particles.

Table 6.5: Effect of homogenization cycle on particle size and entrapment efficiency of LH-SLNs

Homogenization cycle	Particle size (nm)	Entrapment efficiency (%)
1	305.2±6.1	79.30±2.07
3	228.7±7.7	76.10±1.90
5	155.3±4.2	75.72±3.15
7	128.4±3.9	71.10±4.10
9	212.4±3.1	74.50±3.25
11	348.2±4.5	71.10±2.80

6.12.3.2 Influence of formulation variables

6.12.3.2.1 Influence of lipid concentration

It was observed that lipid concentration had prominent effect on both PS and EE. As lipid concentration was increased from 5 to 12.5%, the PS was gradually increased (Table 6.6). Higher lipid contents increased the viscosity, and thereby droplet disruption would be more difficult (15). A relative increase in the turbulent viscous mechanism over the turbulent inertial mechanism may have occured when increasing the volume fraction of dispersed phase, and hence an increase in droplet size (16). Another reason might be the viscosity of dispersion increases with dispersed-oil phase mass fraction and changes in the rheological behaviors of the fluids can occur. As lipid concentration increased the flow behavior changed from newtonian to shear thickning which could lead to formation of aggregates (13). The EE was also increased with increase in lipid concentration because more lipid would be available to encapsulate drug which increased EE.

Table 6.6: Effect of lipid concentration on particle size and entrapment efficiency of LH-SLNs

Lipid concentration (%)	Particle size (nm)	Entrapment efficiency (%)
5	110.7±4.7	34.06±4.14
7.5	127.6±5.4	59.20±3.90
10	159.3±3.8	75.15±2.50
12.5	203.4±2.9	83.45±3.10

6.12.3.2.2 Influence of surfactant concentration

The surfactant also greatly influenced the particle size of formulation by causing stabilization of particles. It was observed that as surfactant concentration was increased from 0.5% to 5%, particle size was gradually decreased from 297.5 nm to 110.5 nm (Table 6.7). At higher surfactant concentration, more amount of surfactant will be available to reduce interfacial tension between two phases, enabling the lipid to become efficiently emulsified in the aqueous phase, and stabilize the nano-droplets and prevent their coalescence. As surfactant concentration increased from 0.5% to 2.5%, entrapment efficiency was found to be increased. Further increase in surfactant concentration from 2.5 % to 5% reduced entrapment efficiency to 58.50% which might be due to higher surfactant concentration of surfactant solubilized drug in the micelles in aqueous phase, leading to reduced entrapment efficiency.

Table 6.7: Effect of surfactant concentration on particle size and entrapment efficiency of LH-SLNs

Surfactant concentration (%)	Particle size (nm)	Entrapment efficiency (%)
0.5	297.5±2.9	41.20±3.00
1	251.3±2.1	54.24±2.74
2	217.9±3.7	62.40±4.21
2.5	155.1±3.1	75.30±3.80
5	110.5±1.8	58.50±4.13

6.12.3.2.4 Type of surfactant

Different surfactants were tried to prepare SLNs and it was observed that particle size increased as follows (Table 6.8): Tween 80>Poloxamer 188> Tween 80: Poloxamer 188> Sodium deooxycholate> Poloxamer 188: TPGS>Poloxamer 188: Sodium deoxycholate. This might be because combination of surfactants helps in reducing interfacial tension more efficiently and helps in stabilization of nano-droplets.

There was insignificant difference in entrapment efficiency among batches prepared using different surfactants. Entrapment efficiency increased as follows: Poloxamer 188: Sodium deoxycholate> Poloxamer 188> Poloxamer 188:TPGS> Tween 80> Sodium deoxycholate> Tween 80:Poloxamer 188.

It is also reported that combination of ionic and non-ionic stabilizers is preferred for emulsification technology; therefore, combination of ionic and non-ionic surfactants may provide SLNs with special properties due to their steric and electostatic effects. Hence, combination of Poloxamer and sodium deoxycholate was selected as surfactant.

Table 6.8: Effect of type of surfactant on particle size and entrapment efficiency of LH-SLNs

Type of surfactant	Particle size (nm)	Entrapment efficiency (%)
Poloxamer 188	307.9±6.9	72.03±3.72
Sodium deoxycholate	198.1±5.5	67.97±3.29
Tween 80	394.2±3.6	70.78±5.62
Poloxamer 188: Sodium deoxycholate	155.5±4.9	77.32±2.76
Tween 80: Poloxamer 188	292.3±3.7	62.34±4.33
Poloxamer 188:TPGS	210.7±4.2	70.61±5.20

6.12.3.2.5 Concentration of sodium deoxycholate

It was observed that as the sodium deoxycholate concentration increased, both particle size and entrapment efficiency was decreased (Table 6.9). It was reported that critical micelle concentration (CMC) of TPGS is 0.25% w/v (17). Therefore, with increase in concentration from 0.125% to 0.25%, drug will get diffused out from nanodroplets and solubilize in micelles; so entrapment efficiency was reduced.

Table 6.9: Effect of sodium deoxycholate concentration on particle size and entrapment efficiency of LH-SLNs

Sodium deoxycholate concentration (%)	Particle size (nm)	Entrapment efficiency (%)
0.1	121.2±4.3	77.21±1.93
0.125	117.4±2.7	76.91±4.27
0.250	106.2±2.4	68.93±3.51

From the results of preliminary optimization, following range of variables were selected for screening design PBD (Table 6.10).

Table 6.10: Values of variables selected for PBD after preliminary optimization of LH-SLNs

PARAMETERS	VALUE	
	-1	+1
Lipid concentration (%)	7.5	12.5
Surfactant concentration (%)	1	2.5
Concentration of sodium deoxycholate (%)	0.1	0.25
Homogenization Speed (rpm)	8000	12000
Homogenization time (min)	1	5
Homogenization pressure (bar)	400	1000
Homogenization cycle	3	9

6.12.4 SCREENING DESIGN: PLACKETT BURMAN DESIGN (PBD)

A screening experimental design minimizes the number of experiments required to identify the most critical factors affecting the response. PBD allows identifying critical factors wits PBD are shown in table 6.11.

Table 6.11: PBD experimental runs of LH- SLNs

LC* (%)	SC* (%)	Sod deoxy Conc (%)	HS* (rpm)	HT* (min)	HP* (bar)	HC*	PS* (nm)	EE* (%)
12.5	2.5	0.25	8000	5	1000	3	299.7±3.4	67.98±2.50
12.5	2.5	0.1	12000	1	400	3	452.3±7.3	78.65±1.89
12.5	2.5	0.1	12000	5	400	9	312.3±4.8	70.56±2.15
7.5	2.5	0.25	12000	1	1000	9	101.2±3.9	49.23±3.20
12.5	1	0.25	8000	1	400	9	351.2±5.5	57.89±2.81
7.5	1	0.1	8000	1	400	3	267.9±6.7	59.10±2.42
12.5	1	0.25	12000	1	1000	3	265.1±2.3	67.34±3.89
12.5	1	0.1	8000	5	1000	9	210.2±5.1	51.45±4.12
7.5	2.5	0.1	8000	1	1000	9	89.2±6.2	44.34±1.20
7.5	2.5	0.25	8000	5	400	3	292.3±5.9	62.23±3.85
7.5	1	0.25	12000	5	400	9	208.2±3.7	57.32±3.27
7.5	1	0.1	12000	5	1000	3	142.3±3.1	46.54±4.20

*Abbreviations: LC: lipid concentration, SC: surfactant concentration, HS: Homogenization speed, HT: Homogenization time, HP: Homogenization pressure, HC: Homogenization cycle, PS: Particle size, %EE: %Entrapment efficiency

6.12.4.1 Influence of various factors on particle size

Seven high risk factors were identified in a risk analysis study to have potential impact on SLN particle size. As shown in table 6.12 for PS, most significant factors were lipid concentration, homogenization pressure and homogenization cycle ($p<0.05$) relative to other factors. The magnitude of coefficients indicates its effect on response. A positive effect value indicates an effect

that favors the response, and a negative value represents an inverse relationship between the response and the factor. Lipid concentration had positive and homogenization speed and pressure had negative influence on PS. Further analysis using ANOVA indicated a significant effect ($p=0.003$) of variables on the response ($p < 0.05$).

Table 6.12: Estimated effects and coefficients for particle size (coded units) of LH-SLNs

Term	Coef	Std error Coef	T	P
Constant	203.18	57.70	3.52	0.024
Lipid conc	26.323	2.872	9.17	0.001
Surfactant conc	11.344	9.574	1.18	0.302
Sod deoxycholate conc	48.33	95.74	0.50	0.640
Homogenization speed	-0.001212	0.003590	-0.34	0.753
Homogenization time	-2.579	3.590	-0.72	0.512
Homogenization pressure	-0.21569	0.02393	-9.01	0.001
Homogenization cycle	-12.425	2.393	-5.19	0.007

Main effect plot for particle size (Figure 6.4) indictes that PS was highly influenced by lipid concentration, homogenization pressure and homogenization cycle whereas other factors had negligible effect on PS.

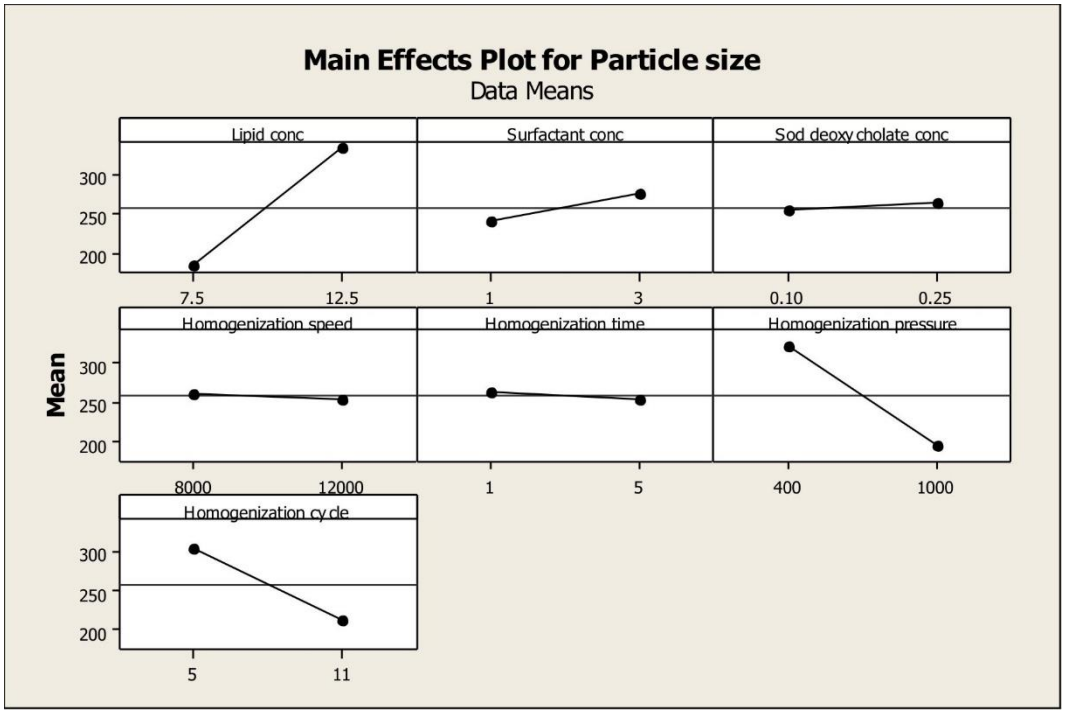

Figure 6.4: Main effect plot for particle size of LH-SLNs

Pareto chart indicates that any effects that extend beyond the reference line are considered as significant. Here, the chart (Figure 6.5a) shows that lipid concentration, homogenization pressure and homogenization cycle are beyond the reference line and

were considered as critical variables for particle size. Half normal plot displays the absolute value of each factor. Points that are away from the zero usually indicate significant effects (Figure 6.5b). Normal plot indicated that lipid concentration had positive whereas homogenization pressure and homogenization cycle had negative effect on particle size (Figure 6.5c). This result is in accordance with effect analysis.

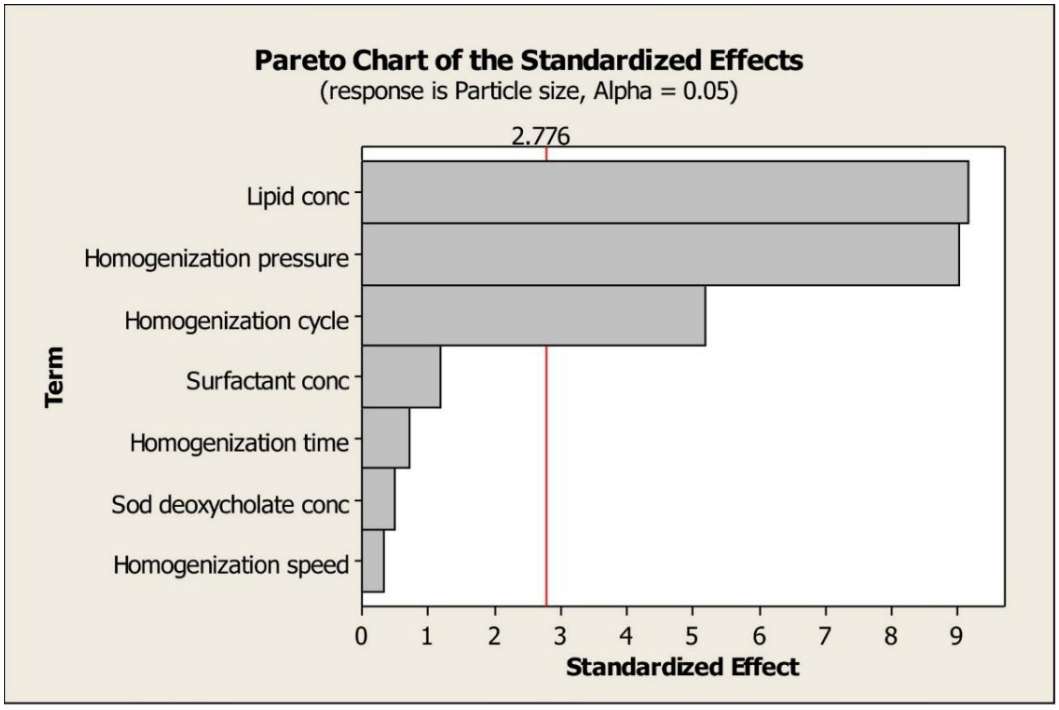

(a)

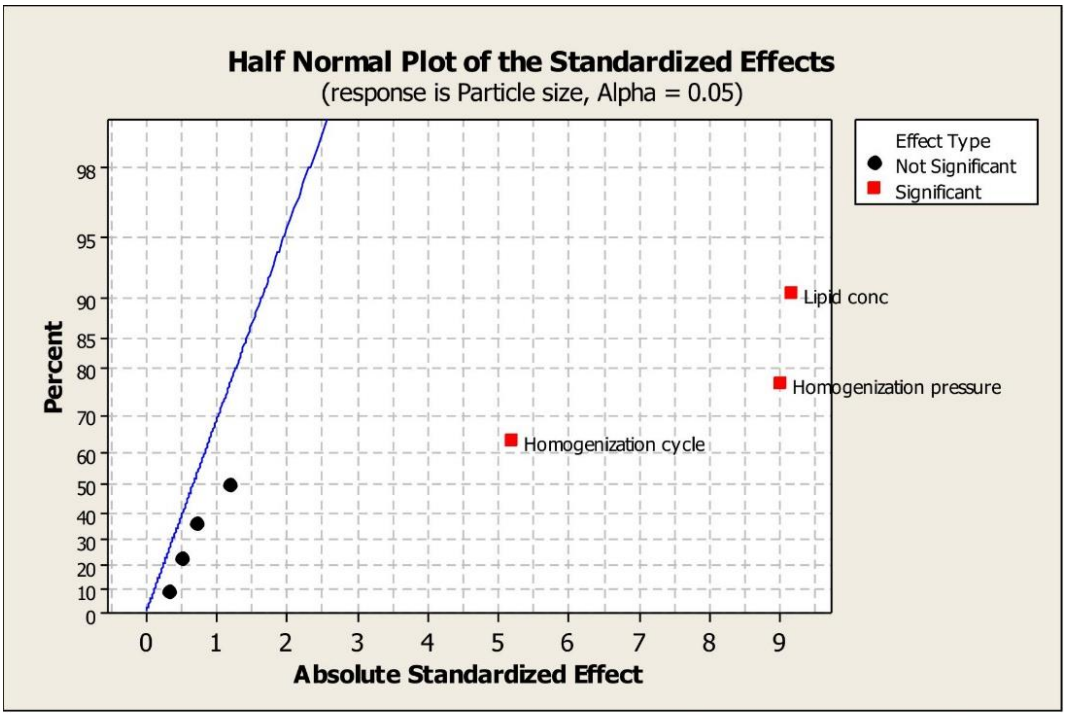

(b)

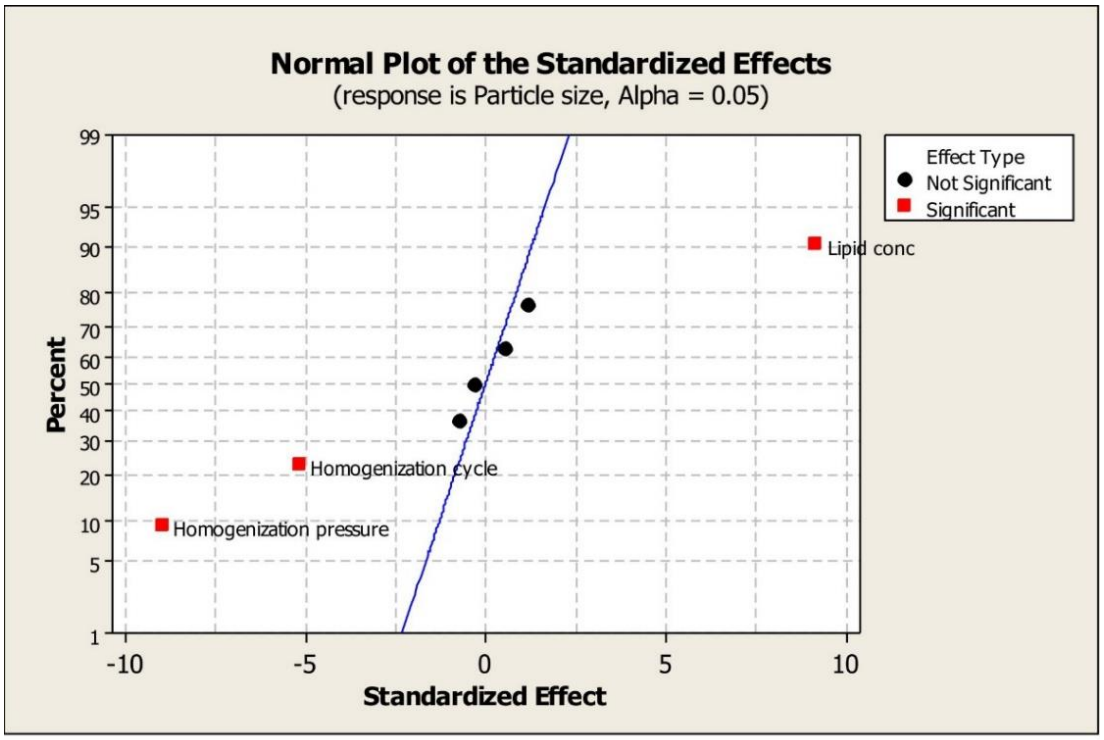

(c)

Figure 6.5: (a) Pareto chart (b) Half normal plot and (c) Normal plot for particle size of LH-SLNs

6.12.4.2 Influence of various factors on entrapment efficiency

Seven high risk factors were identified in a risk analysis study to have potential impact on SLN entrapment efficiency. As shown in table 6.13 for EE, most significant factors were lipid concentration, homogenization pressure and homogenization cycle ($p<0.05$) relative to other factors. Lipid concentration had positive and homogenization speed and pressure had negative influence on EE. Further analysis using ANOVA indicated a significant effect ($p=0.022$) of variables on the response ($p<0.05$).

Table 6.13: Estimated effects and coefficients for entrapment efficiency (coded units) of LH-SLNs

Term	Coef	Std error Coef	T	P
Constant	38.330	9.584	4.00	0.016
Lipid conc	2.5037	0.4710	5.32	0.006
Surfactant conc	2.779	1.178	2.36	0.078
Sod deoxycholate conc	12.61	15.70	0.80	0.467
Homogenization speed	0.0011104	0.0005888	1.89	0.132
Homogenization time	-0.0196	0.5888	-0.03	0.975
Homogenization pressure	-0.016353	0.003925	-4.17	0.014
Homogenization cycle	-1.4181	0.3925	-3.61	0.022

Main effects plot for entrapment efficiency (Figure 6.6) indictes that EE was highly influenced by lipid concentration, homogenization pressure and homogenization cycle whereas other factors had negligible effect on EE.

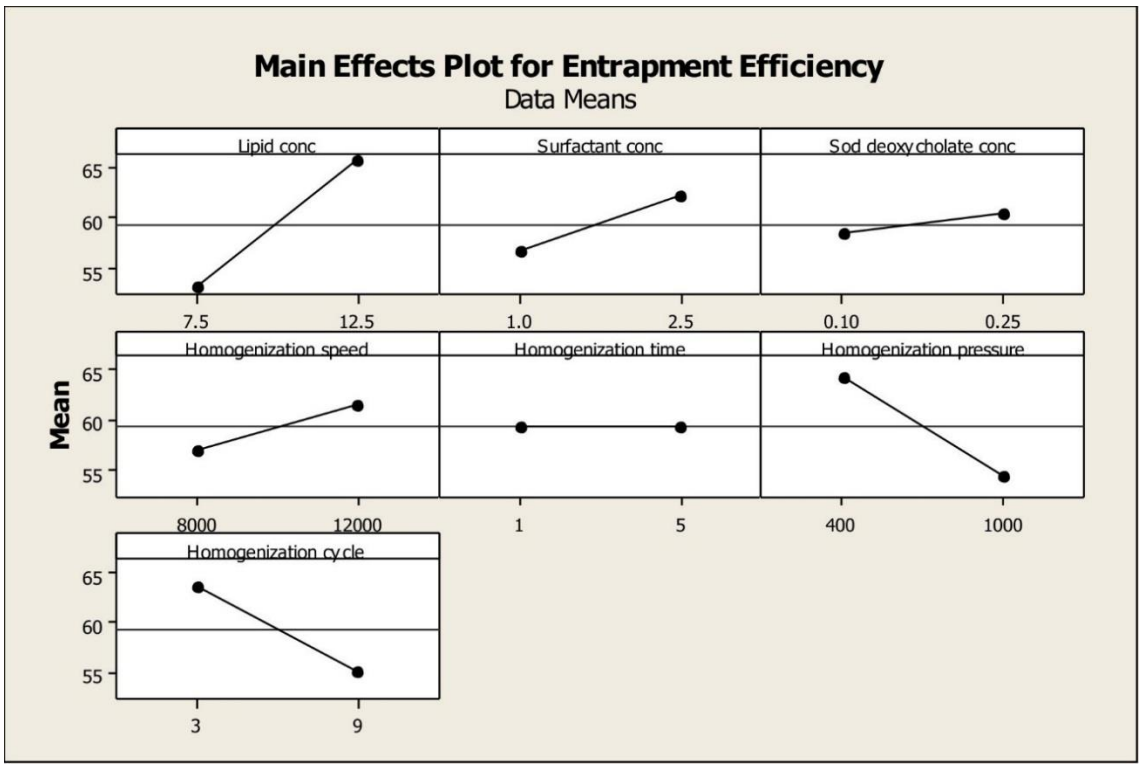

Figure 6.6: Main effect plot for entrapment efficiency of LH-SLNs

Pareto chart indicates (Figure 6.7a) that lipid concentration, homogenization pressure and homogenization cycle are beyond the reference line and were considered as critical variables for entrapment efficiency. Normal plot indicated that lipid concentration has positive effect whereas homogenization pressure and homogenization cycle had negative effect on entrapment efficiency (Figure 6.7c).

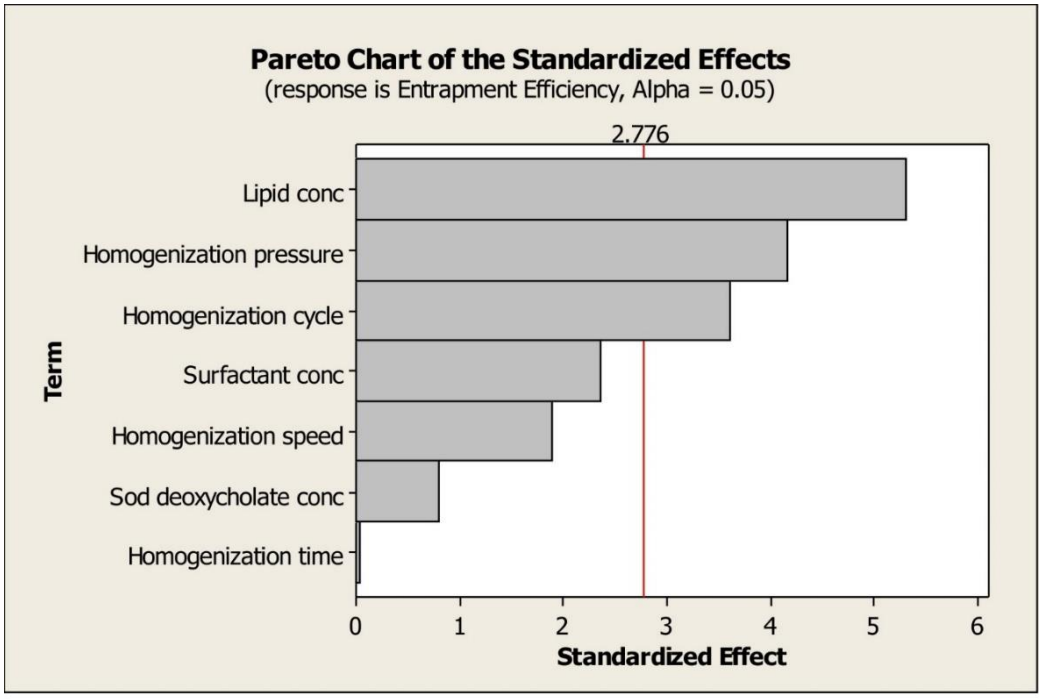

(a)

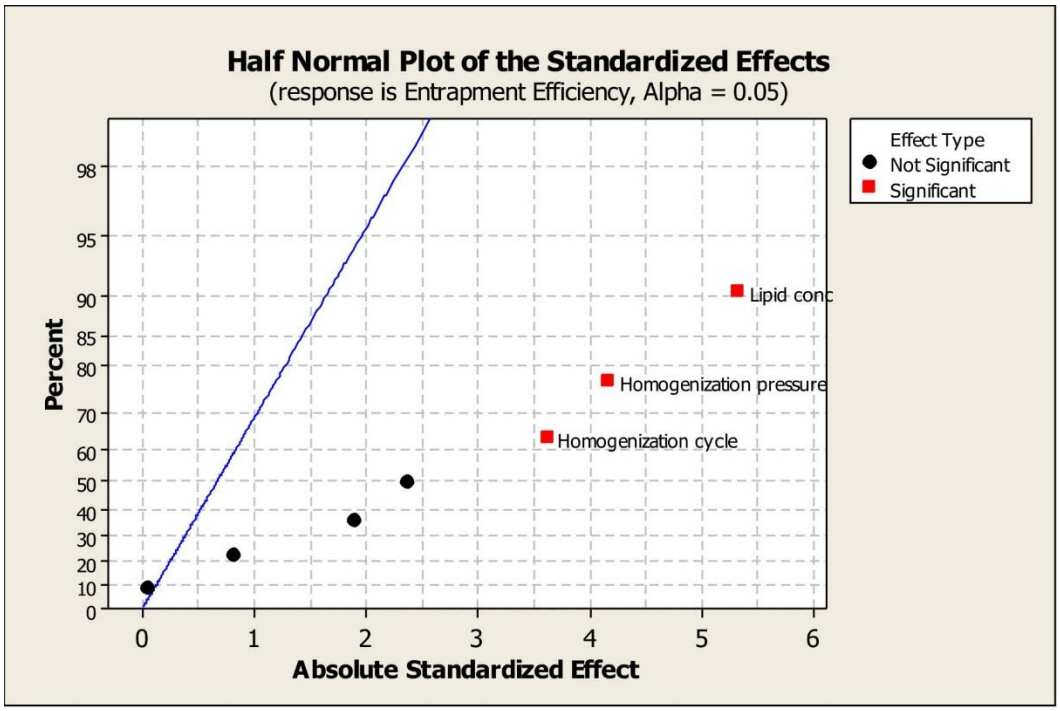

(b)

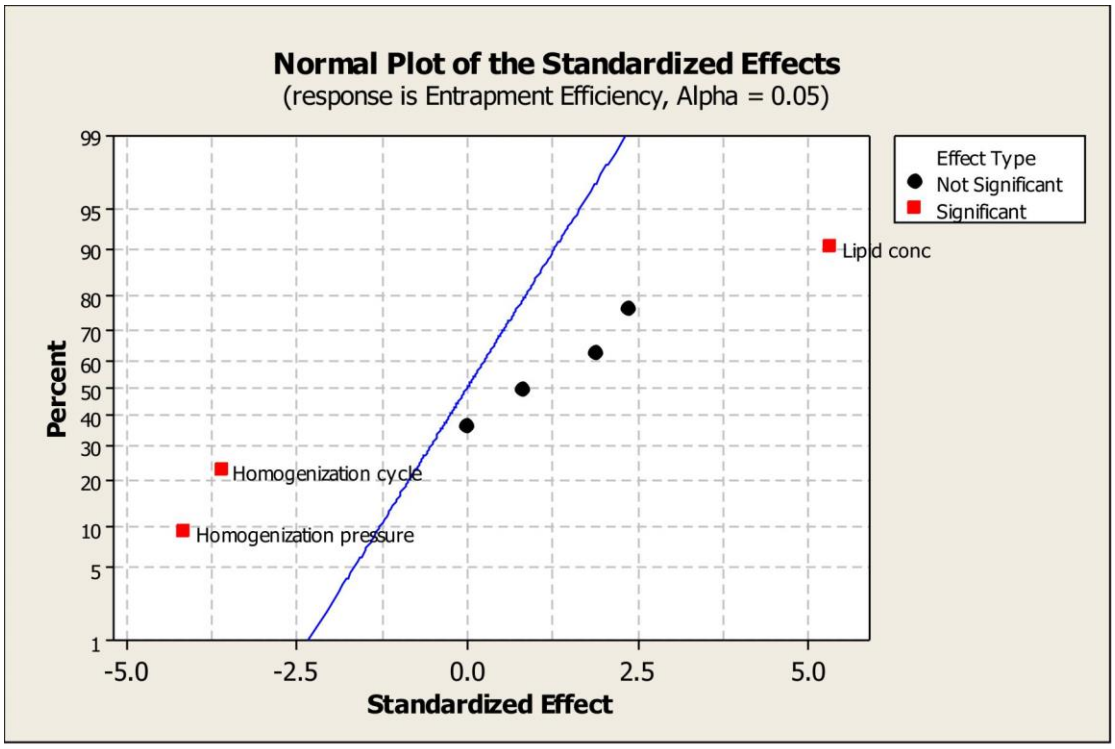

(c)

Figure 6.7 : (a) Pareto chart (b) Half normal plot and (c) Normal plot for entrapment efficiency of LH-SLNs

6.12.5 Optimization using BBD

Following the screening study, the three most significant factors (lipid concentration, homogenization pressure and homogenization cycle) were evaluated using a response surface method. In contrast to the screening design, where the generated model is only sufficient for qualitative determination of the main effects, the response surface design would allow generation of a more predictive model. The accuracy of the response surface design is much higher than even a full factorial design in terms of prediction variance (18). The results of BBD are shown in table 6.14.

Table 6.14: Box Behnken Design experimental runs of LH-SLNs

Sr. No.	X_1 (%)	X_2 (bar)	X_3	Y_1 (nm)	Y_2 (%)
1	10	600	7	138.2±2.8	80.42±3.45
2	7.5	400	7	146.3±3.4	53.65±2.90
3	10	400	5	184.3±3.9	79.34±1.87
4	10	600	7	154.2±4.2	76.1±1.65
5	7.5	600	5	114.5±4.0	58.98±2.20
6	10	800	9	110.6±2.1	55.04±2.56
7	10	400	9	176.8±1.7	81.67±4.10
8	12.5	800	7	191.3±1.9	74.6±2.10
9	12.5	600	5	253.7±2.6	80.77±3.20
10	12.5	600	9	205.7±5.2	81.09±1.55
11	10	600	7	139.7±5.6	78.41±1.87
12	7.5	600	9	104.2±3.9	41.43±2.67
13	10	800	5	102.3±4.6	59.22±2.51
14	12.5	400	7	388.2±3.7	79.69±3.01
15	7.5	800	7	101.2±4.1	32.6±3.57

6.12.5.1 Influence of independent variables on particle size

The full model polynomial equation (Equation 6.3) was generated by the statistical analysis of the results:

$$Y_1 = 144.03 + 71.59X_1 - 48.78X_2 - 7.19X_3 - 37.95X_1X_2 - 9.42X_1X_3 + 3.95X_2X_3 + 44.37X_1^2 + 18.35X_2^2 - 18.88X_3^2 \ldots\ldots\ldots\ldots\ldots\ldots\ldots Equation\ 6.3$$

Non-significant terms were rejected (P > 0.05) to obtain reduced model as follows (Equation 6.4):

$$Y_1 = 143.73 + 71.59X_1 - 48.78X_2 - 37.95X_1X_2 + 44.41X_1^2 \ldots\ldots\ldots\ldots\ldots\ldots\ldots Equation\ 6.4$$

Table 6.15: Effect tests analysis of independent variables on particle size of LH-SLNs

	Sum of Squares	**df**	**Mean square**	**F Value**	**p-value prob>F**
Model	76756.58	9	8528.51	15.59	0.0037
X_1	40998.16	1	40998.16	74.96	0.0003
X_2	19032.01	1	19032.01	34.80	0.0020
X_3	413.28	1	413.28	0.76	0.4244
X_1X_2	5760.81	1	5760.81	10.53	0.0228
X_1X_3	355.32	1	355.32	0.65	0.4568
X_2X_3	62.41	1	62.41	0.11	0.7492
X_1^2	7269.31	1	7269.31	13.29	0.0148
X_2^2	1242.72	1	1242.72	2.27	0.1921
X_3^2	1316.02	1	1316.02	2.41	0.1815
Residual	2734.53	5	546.91		
Lack of Fit	2578.37	3	859.46	11.01	0.0844
Pure Error	156.17	2	78.08		
Cor Total	79491.12	14			

Based on the P value (Table 6.15), X_1, X_2, X_1X_2 and X_{12} factors were found to be significant ($p<0.05$) and all other factors were found to be non significant. A positive value in polynomial equations corresponds to an effect that favors the optimization, while a negative value corresponds to an inverse relationship between the factor and the response (19).

In accordance with the above stated equation for PS, increase in lipid concentration increased PS. This could be due to the higher lipid contents increased the viscosity which made droplet disruption more difficult so PS increased. Also, as the homogenization pressure increased, strong decrease in PS was observed. More energy would be provided at higher pressure for particle breakdown which ultimately decreased PS. The contour and three-dimensional (3D) response surface graphs which depict the interaction effects of the independent variables on the responses are shown in figure 6.8 to 6.10.

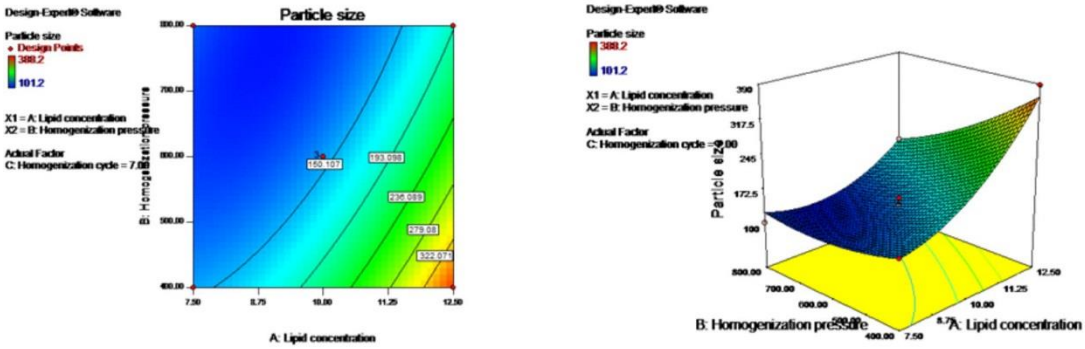

(a) (b)

Figure 6.8 : (a) Contour and (b) Response surface plot showing effect of lipid concentration and homogenization pressure on particle size of LH-SLNs

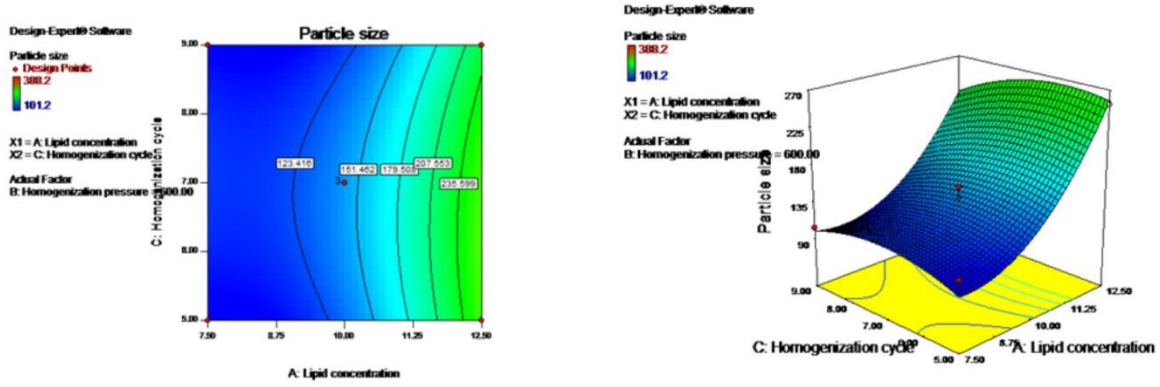

(a) (b)

Figure 6.9 : (a) Contour and (b) Response surface plot showing effect of lipid concentration and homogenization cycle on particle size of LH-SLNs

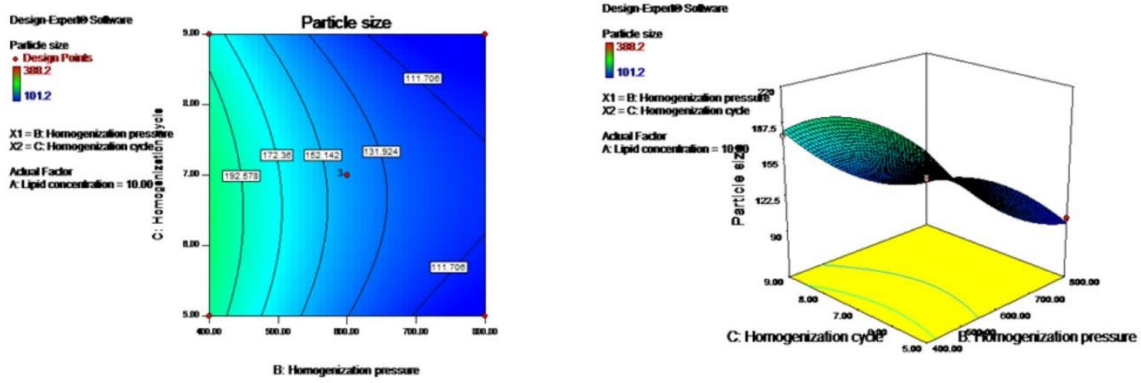

(a) (b)

Figure 6.10 : (a) Contour and (b) Response surface plot showing effect of homogenization pressure and homogenization cycle on particle size of LH-SLNs

6.12.5.2 Influence of independent variables on entrapment efficiency

The following full model (Equation 6.5) and reduced model (Equation 6.6) polynomial equations were generated by the statistical analysis of the results:

Full model equation:

$$Y_2 = 78.31 + 16.19X_1 - 9.11X_2 - 2.38X_3 + 3.99X_1X_2 + 4.47X_1X_3 - 1.63X_2X_3 - 10.71X_1^2 - 7.46X_2^2 - 2.03X_3^2 \ldots\ldots\ldots\ldots\ldots\ldots Equation\ 6.5$$

Reduced model equation:

$$Y_2 = 77.06 + 16.19X_1 - 9.11X_2 - 10.56X_1^2 - 7.31X_2^2 \ldots\ldots\ldots\ldots\ldots\ldots Equation\ 6.6$$

Table 6.16: Effect tests analysis of independent variables on entrapment efficiency of LH-SLNs

Source	Sum of Squares	df	Mean square	F Value	p-value prob>F
Model	3549.10	9	394.34	20.24	0.0020
X_1	2095.96	1	2095.96	107.55	0.0001
X_2	664.12	1	664.12	34.08	0.0021
X_3	45.51	1	45.51	2.34	0.1870
X_1X_2	63.68	1	63.68	3.27	0.1305
X_1X_3	79.83	1	79.83	4.10	0.0989
X_2X_3	10.60	1	10.60	0.54	0.4940
X_1^2	423.72	1	423.72	21.74	0.0055
X_2^2	205.62	1	205.62	10.55	0.0227
X_3^2	15.22	1	15.22	0.78	0.4174
Residual	97.44	5	19.49		
Lack of Fit	88.09	3	29.36	6.28	0.1404
Pure Error	9.35	2	4.67		
Cor Total	3646.54	14			

Based on the p value (Table 6.16), X_1, X_2, X_{12} and X_{22} factors were found to be most significant ($p<0.05$) as compared to other factors.The results reveal that X1 had postitve effect on EE i.e. an increase in concentration of total lipid resulted in increased EE. The possible reason behind this could be that higher lipid content prevents the escape of drug to outer milieu by effectively enclosing it (19). However, X_2 had negavtive influence on EE which could be due to an increase in the pressure led to a significant decrease in EE which might be again due to the decrease in particle size. This effect of independent variables on EE can further be visualized from contour and response surface plots (Figure 6.11 to 6.13).

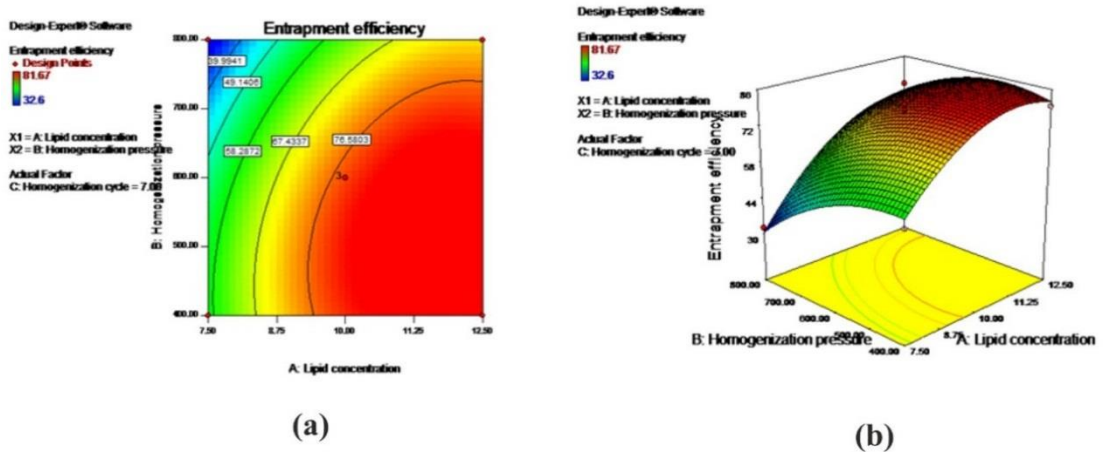

Figure 6.11: (a) Contour and (b) Response surface plot showing effect of lipid concentration and homogenization pressure on entrapment efficiency of LH-SLNs

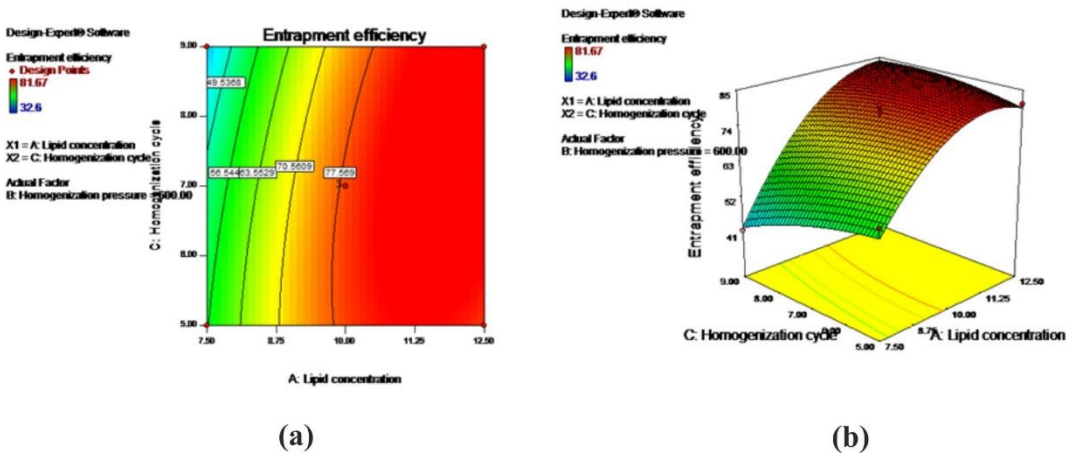

Figure 6.12: (a) Contour and (b) Response surface plot showing effect of lipid concentration and homogenization cycle on entrapment efficiency of LH-SLNs

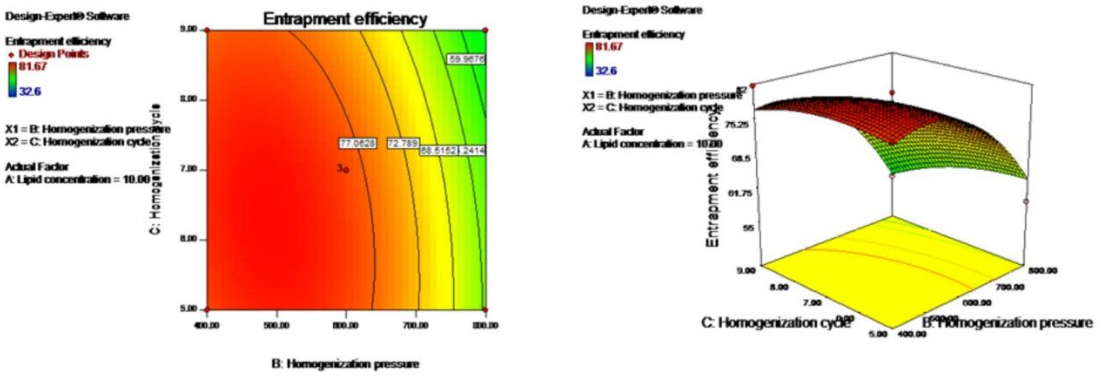

Figure 6. 13: (a) Contour and (b) Response surface plot showing effect of homogenization pressure and homogenization cycle on entrapment efficiency of LH-SLNs

6.12.5.3 Statistical analysis of designed experiment

The adequacy of the quadratic model was verified by ANOVA, lack of fit and multiple correlation coefficient (R^2) tests provided by Design- Expert software. The results of ANOVA showed that p value for response PS and EE was found to be 0.0037 and 0.0020 respectively. Thus it can be concluded that all the responses fitted the model well ($p<0.05$) Moreover, the lack of fit test is another good statistical parameter for checking the fitness of the model. It compares the residual error with the pure error from the replicated design points. A model with a significant lack-of-fit (Prob>F value 0.10) lacks prediction efficiency, so a non-significant lack of- fit value in the model is highly desirable. The lack of fit value for PS and EE was found to be 0.0844 and 0.1404 respectively. All of these responses fitted in the cubic model showed a non-significant lack-of-fit ($p>0.1$), proving the adequacy of the model fit. Furthermore, the multiple regression analysis for the quadratic model is shown as R^2 value, which signifies the measure of the amount of variation around the mean explained by the model. In our study, the R^2 values for the responses PS and EE were 0.9656 and 0.9733 respectively.

6.12.5.4 Validation of design

Check point batch was prepared as suggested by software by selecting constraints for PS and EE to be minimized and maximized respectively. The predicted and experimental value for the responses are shown in table 6.17. The percentage prediction

error for PS and EE in the check point analysis was found to be very less between pedicted value and experimental value.

Table 6.17: Predicted and observed responses for check point batch of LH-SLNs

Response	Predicted value	Experimental value	Percentage prediction error
Y_1 (nm)	126.07	128.5±2.20	-1.93
Y_2 (%)	77.68	79.20±1.20	-1.96

The concept behind a desirability function using multi-response optimization process is to transform multi-response into single response using mathematical calculation. The desirability for the selected quadratic model was found to be 0.916 (Figure 6.14) indicating accurate and reliable approach in the optimization process.

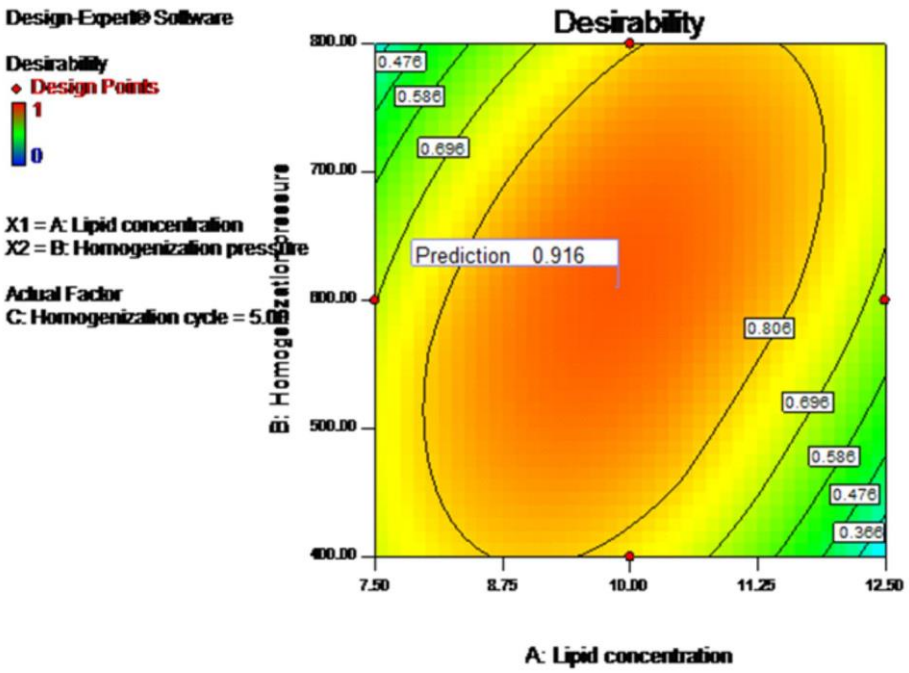

Figure 6.14: Desirability plot of optimized batch of LH-SLNs

6.12.5.5 Analysis of Design Space robustness

The design space was generated using the aforementioned criteria by a graphical-optimization technique. Figure 6.15 portrays the optimal design space region within the requisite knowledge space and location of the optimum formulation within the desired limits. It was observed that value of independent variables outside the design space showed variation in response (Table 6.18). So, it proved that the design space was

sensitive to variation in independent variables. The yellow area showing desired response indicated the robustness of design space.

Table 6.18: Evaluation of sensitivity of obtained design space of LH-SLNs

X_1 (%)	X_2 (bar)	X_3	Y_1 (nm)		Y_2 (%)	
			Predicted	**Observed**	**Predicted**	**Observed**
7.52	513.86	5	105.551	107.7±2.5	60.08	62.20±3.04
9.88	610.30	5	126.06	130.4±1.9	77.68	79.03±2.20
10.19	408.52	5	208.69	213.3±3.5	79.52	78.00±2.00

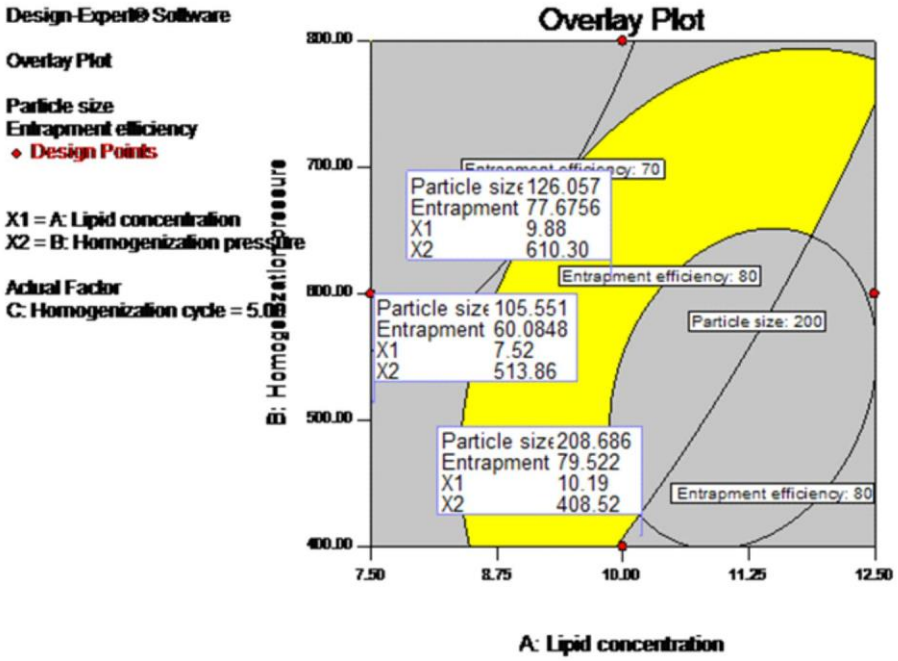

Figure 6.15 : Overlay plot depicting the design space for optimized batch of LH-SLNs

6.13 CHARACTERIZATION

6.13.1 Determination of Particle size

The optimized LH-SLNs were in the nanometric size range, 139.8±5.5 nm (Figure 6.16). The smaller particle size provides large surface area for absorption and thus, can improve its oral performance. It was also reported that particle size below 200 nm promotes lymphatic uptake of SLNs (20). The PDI of the optimized batch of LH loaded SLN was found to be 0.118±0.020 which illustrated unimodel size distribution of particles prepared using HPH.

Results

		Size (d.nm):	% Intensity	Width (d.nm):
Z-Average (d.nm): 139.8	Peak 1:	136.8	100.0	42.63
PdI: 0.118	Peak 2:	0.000	0.0	0.000
Intercept: 0.935	Peak 3:	0.000	0.0	0.000
Result quality : Good				

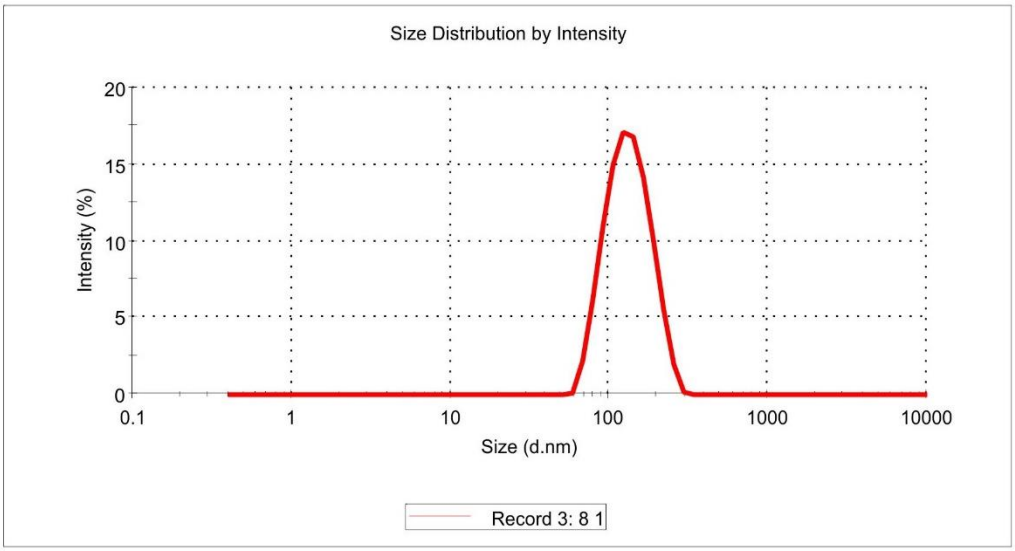

Figure 6.16: Particle size of optimized batch of LH-SLNs

6.13.2 Zeta potential determination

The nature and intensity of the zeta potential value is of importance for predicting the long-term stability of the colloidal system in addition to their interaction with the biological environment (21). The zeta potential of optimized SLNs was found to be -30.8±3.5 mV (Figure 6.17). It was reported that negatively charged carriers show higher lymphatic uptake than neutral or positively charged surfaces, which could be due to the fact that the interstitial matrix contains a net negative charge. Therefore, in the interstitium, anionic carrier particles encounter electrostatic repulsion and move more quickly (22). The net negative surface charge of SLN was attributed to anionic nature of surfactant, sodium deoxycholate used in formulation development which provides strong electrostatic properties (23).

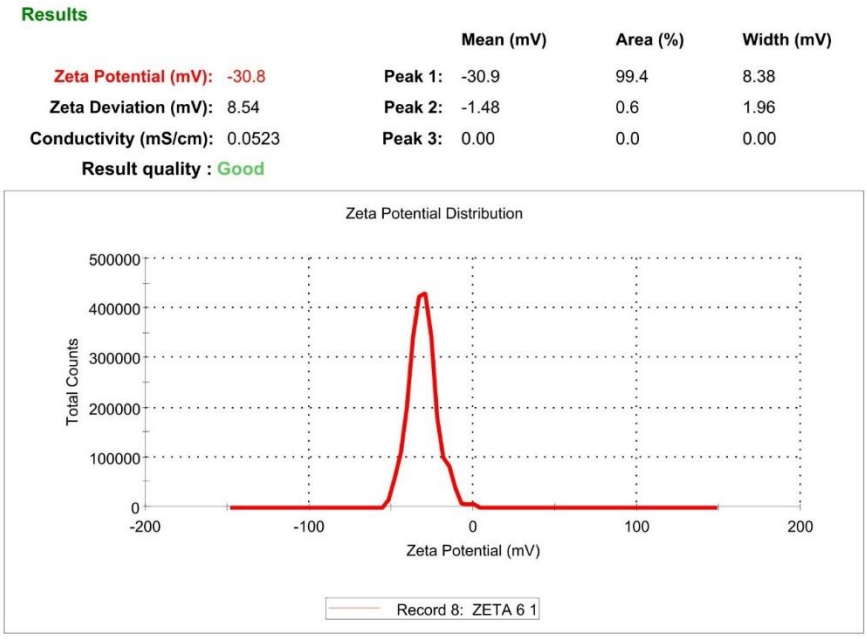

Figure 6.17: Zeta potential of optimized batch of LH-SLNs

6.13.3 Lyophilization of SLN and optimization of cryoprotectant

Since the aqueous SLN dispersion is pliable to physical and chemical stability problems, lyophilization seems to be the promising way to increase the stability of SLN for extended period of time. Furthermore transformation into solid form offers possibilities of incorporating SLN into pellets, tablets and capsules (24). The enhancement ratio of PS was found to be lowest (1.16) for sucrose in 1:3 ratio (Table 6.19).

Table 6.19: : Optimization of cryoprotectants of LH-SLNs

Cryoprotectant	Ratio	Particle size (nm)	PDI	Enhancement ratio
Initial PS	-	139.8±5.5	0.118±0.020	-
Trehalose	1:1	373.7±4.7	0.454±0.052	2.67
	1:2	298.7±3.5	0.343±0.047	2.13
	1:3	256.0±6.7	0.282±0.056	1.83
Sucrose	1:1	317.9±3.0	0.199±0.093	2.27
	1:2	260.3±3.5	0.278±0.010	1.86
	1:3	163.3±5.4	0.136±0.044	1.16
Mannitol	1:1	253.3±8.9	0.317±0.073	1.81
	1:2	313.1±4.9	0.567±0.050	2.24
	1:3	569.0±5.1	0.402±0.027	4.07

6.13.4 Determination of Entrapment efficiency and drug content

The %EE of optimized batch was found to be 79.10± 2.50%. In SLN, the solid lipid provides a crystalline matxrix to entrap more drug. Here the high EE was due to high solubility of drug in GMS which provided sufficient space to entrap drug. Moreover, long chain fatty acids attached to the glyceride resulted in increased accommodation of lipophilic drugs. The total drug content of optimized batch was found to be 99.20±1.2%.

6.13.5 Fourier Transform Infra-red spectroscopy (FTIR)

The IR spectra of LH showed characteristic peaks 2936 cm^{-1}, 2258.0 cm^{-1} and 1687.5 cm^{-1} indicative of C-H stretching, N-H stretching and C=O stretching respectively (Figure 6.18a). The IR spectra of GMS showed characteristic peaks at 2914.44 cm^{-1}, 1730.15 cm^{-1} and 1176.58 cm^{-1} indicative of C-O stretching, C-H stretching and C=O stretching respectively (Figure 6.18b). The FTIR spectra of physical mixture showed all characteristic peaks of LH indicating absence of chemical interaction between lipid and drug (Figure 6.18c). The FTIR spectra of lyophilized LH-SLNs (Figure 6.18d) showed absence of characteristic peaks corresponding to LH but peak corresponding to GMS was present confirming the encapsulation of drug in GMS (19).

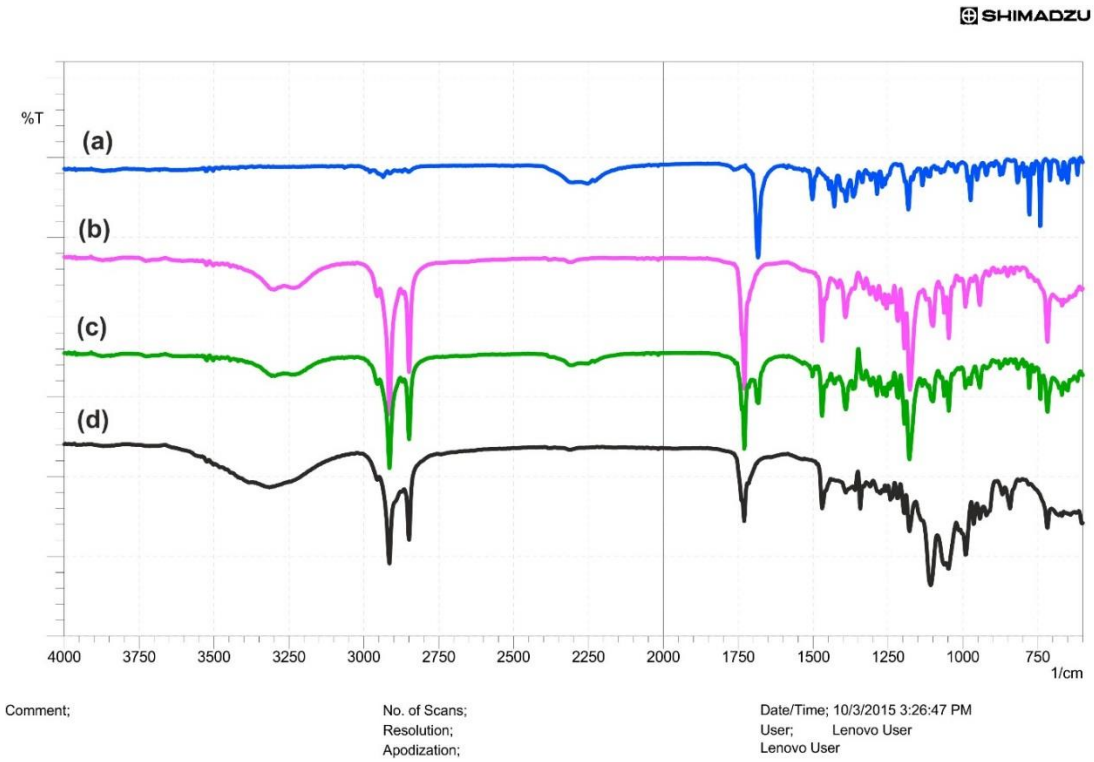

Figure 6.18: FTIR spectrum of (a) LH (b) GMS (c) Physical mixture of LH and GMS and (d) lyophilized LH-SLNs

6.13.6 Differential Scanning Calorimeter (DSC)

The DSC thermograms of bulk LH, GMS, Physical mixture of LH and GMS and lyophilized SLN are shown in figure 6.19. Thermogram of LH and GMS showed endothermic peaks at 272.00 °C and 62.72 °C corresponding to their melting points as depicted in Fig. 6.19a and 6.19b, respectively. The physical mixture of drug and GMS, showed the melting endotherm at 62.74 °C corresponds to melting point of GMS. It showed absence of melting endotherm of drug indicating drug is completely solubilized in lipid. Thermogram of lyophilized LH-SLNs showed endothermic peak at 56.58°C representing the melting point of GMS but the absence of endothermic peak of LH indicates conversion of drug from crystalline to amorphous form in the lipid matrix. The endothermic peak at 182.16 °C corresponds to melting enthalpy of sucrose, a cryoprotectant used for lyophilization of LH loaded SLNs. The phase transition temperature of colloidal dispersions was always much lower than the anhydrous lipid mixtures. The melting points of colloidal systems were distinctly decreased by about 3–8 °C (24). In our study, phase transition temperature of SLN (56.58°C) was lowered than anhydrous physical mixture (62.74 °C). Therefore, lower melting enthalpy value suggest distortion in lattice arrangement in lyophilized SLN. As a result, it can be

concluded that the lipid within the SLNs must be in a less ordered arrangement compared to the pure glyceryl monostearate (14).

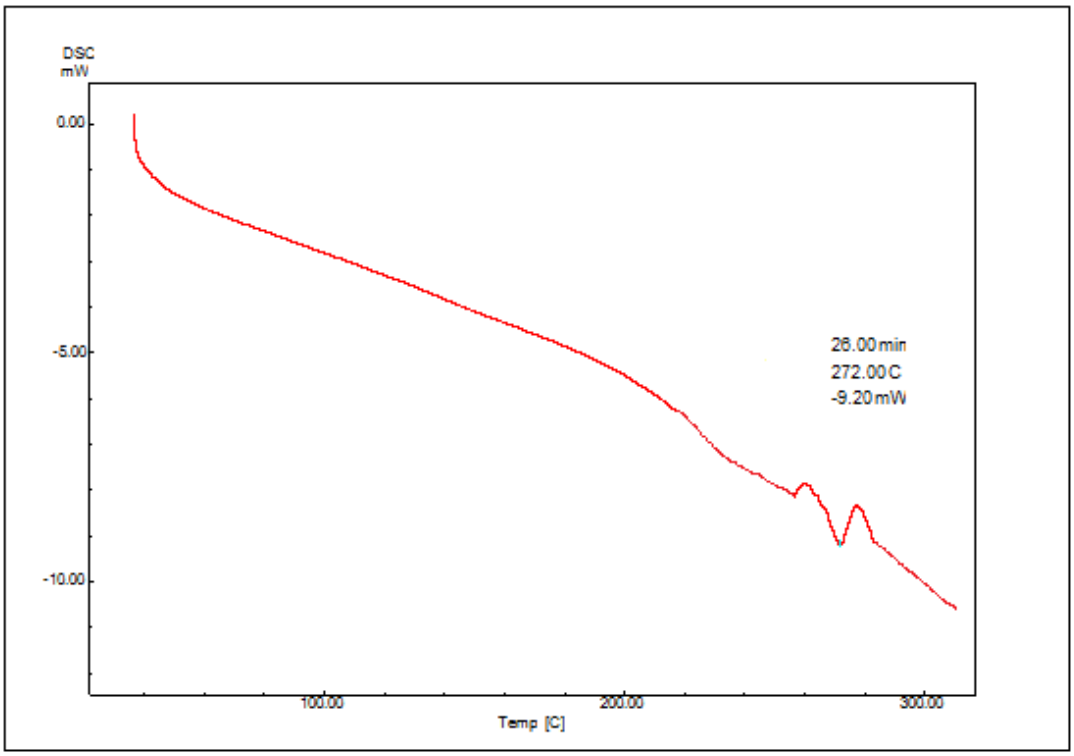

(a)

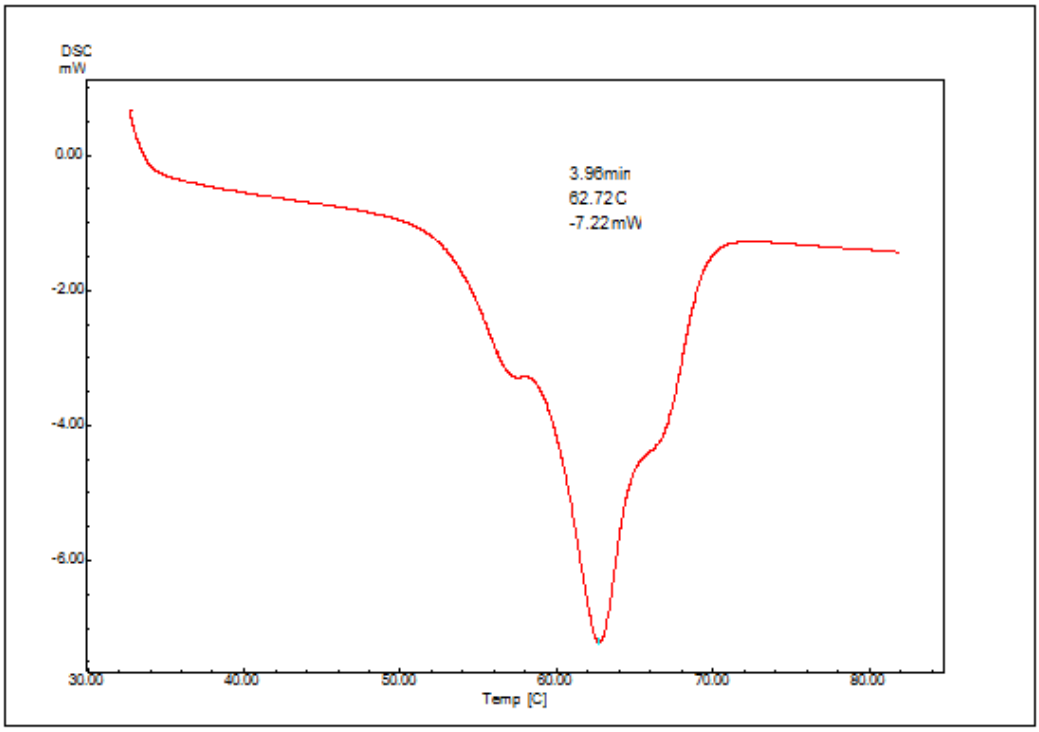

(b)

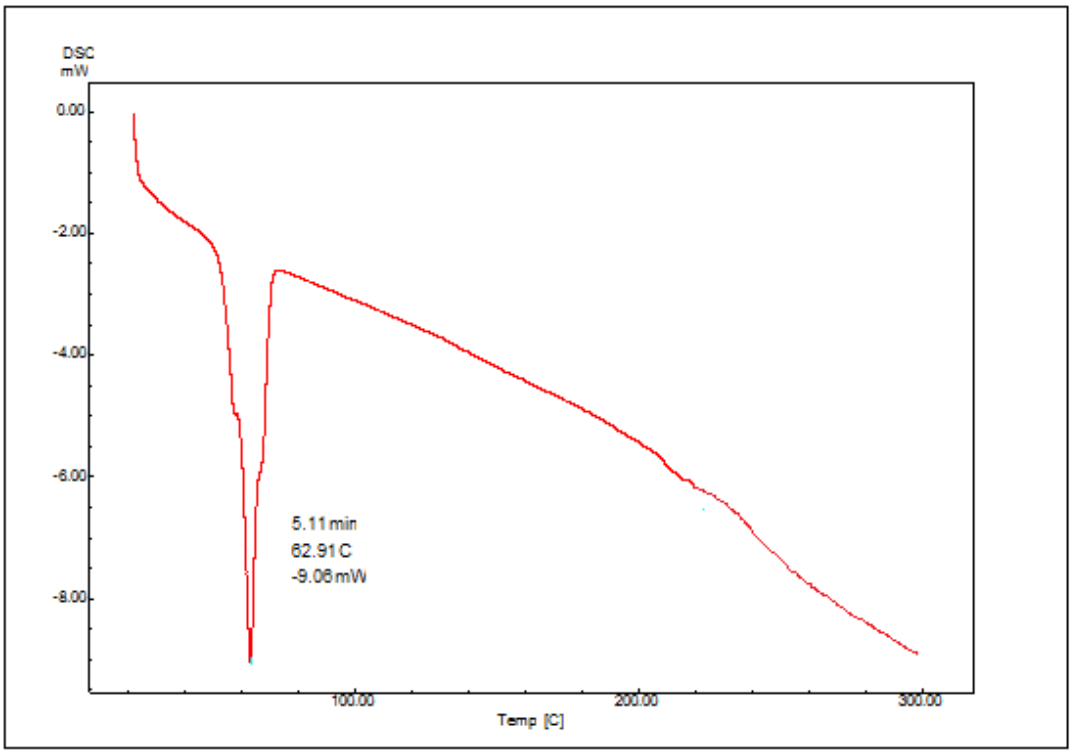

(c)

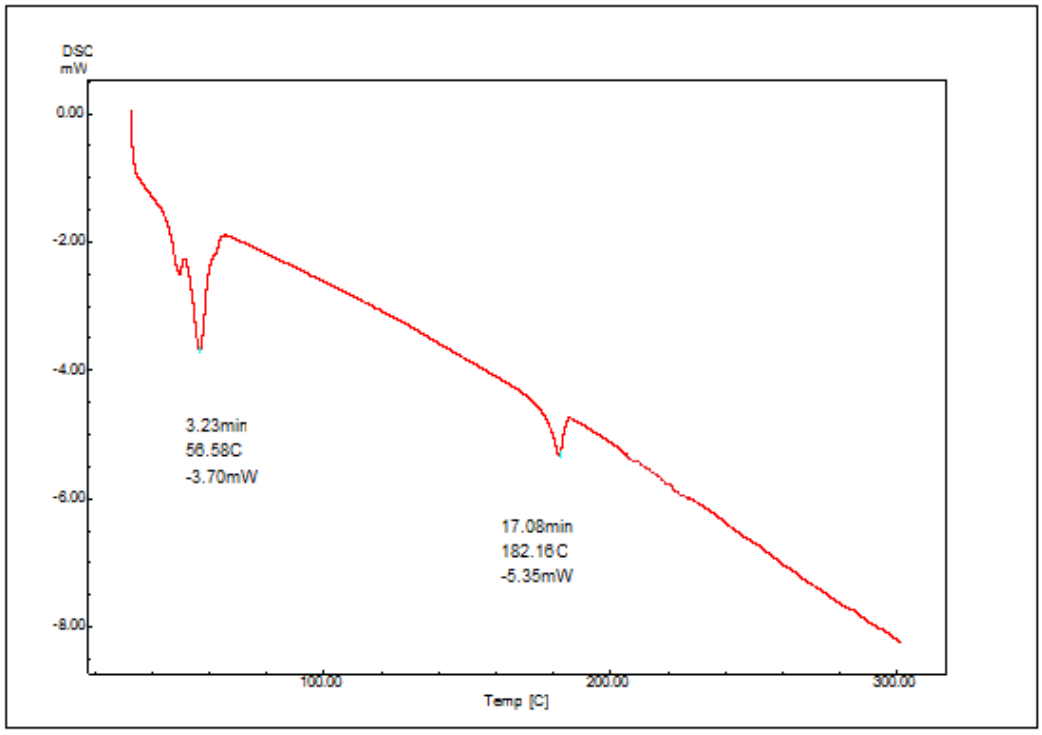

(d)

Figure 6.19: DSC thermogram of (a) LH (b) GMS (c) Physical mixture of LH and GMS (d) lyophilized LH-SLNs

6.13.7 X Ray Diffraction (XRD) study

The XRD study was carried out with support of DSC to verify the reduction in crystalline nature of LH in prepared formulation.

The diffraction pattern of LH (Figure 6.20) showed distinct sharp peak at 2Θ=11.55°, 14.52°, 15.50°, 17.49°, 19.64°, 20.89°, 21.34°, 22.04°, 23.18°, 29.54°, 36.11°, 39.55°and 43.19° indicating crystalline nature of LH. The diffraction pattern of GMS showed peak at 2Θ=19.1°, 22.9°, 29.6°, 36.4°and 39.8°. The characteristic peaks of LH could not be detected in physical mixture of drug and lipid which indicates complete solubilization of drug in the GMS. The degree of crystallinity was compared on the basis of peak intensities. The absence of typical peaks of LH in lyophilized LH-SLNs confirmed the amorphization of drug in lipid matrix. The change in crystallinity of lipid and drug is having the influence on the release of LH from SLNs (24). Therefore, it can be revealed that LH is completely in amorphous state in optimized LH-SLNs formulation with solid lipid. Thus, XRD results support the DSC results.

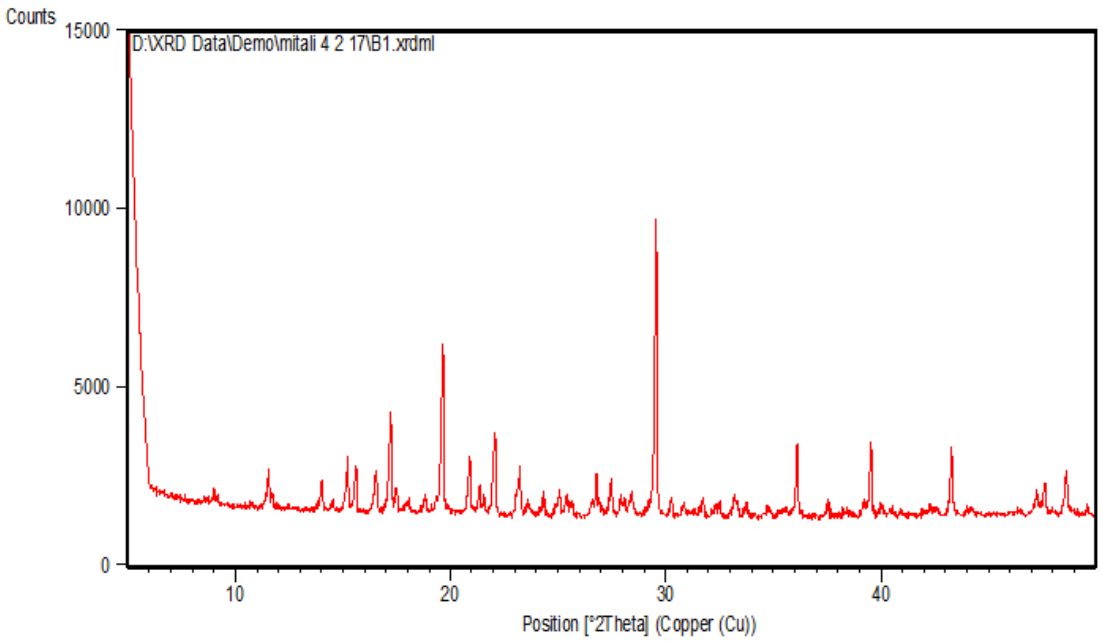

(a)

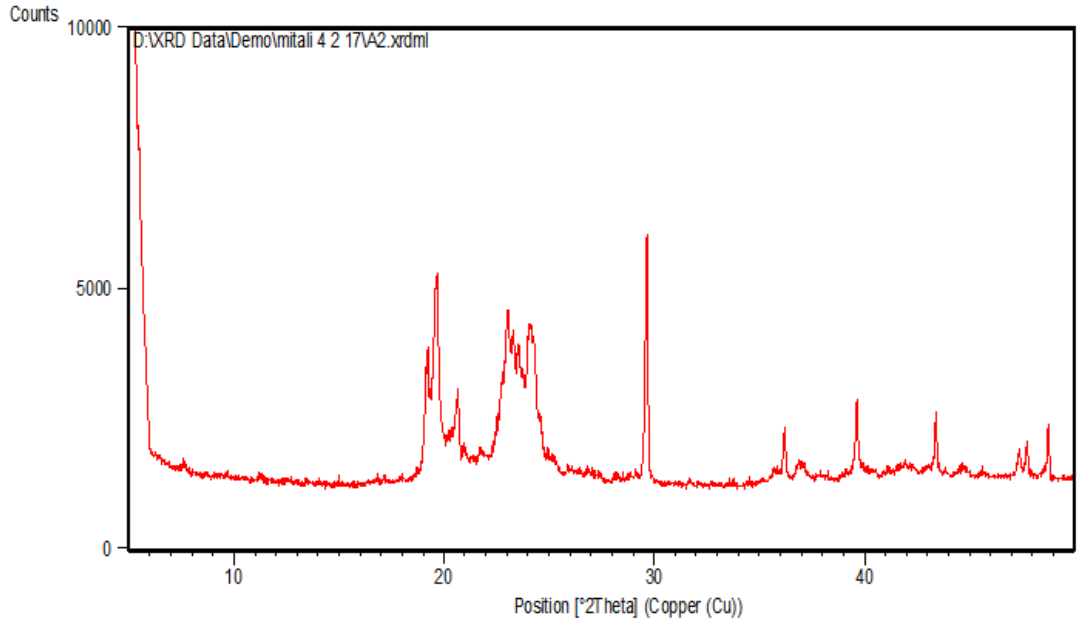
Counts
10000
5000
0
D:\XRD Data\Demo\mitali 4 2 17\A2.xrdml
10
20
30
40
Position [°2Theta] (Copper (Cu))

(b)

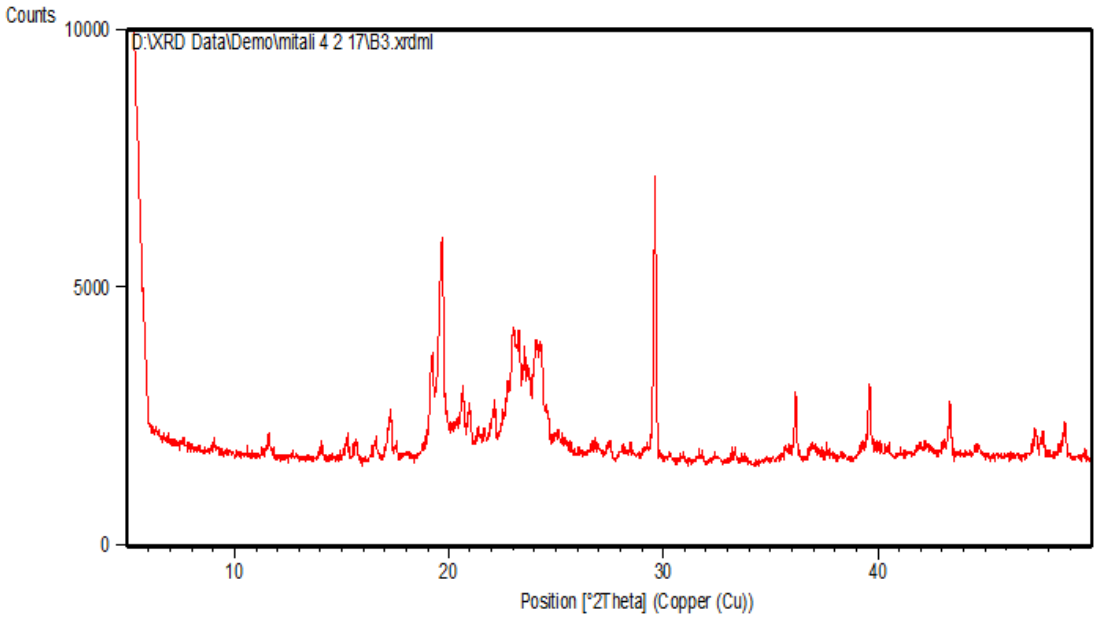
Counts
10000
5000
0
D:\XRD Data\Demo\mitali 4 2 17\B3.xrdml
10
20
30
40
Position [°2Theta] (Copper (Cu))

(c)

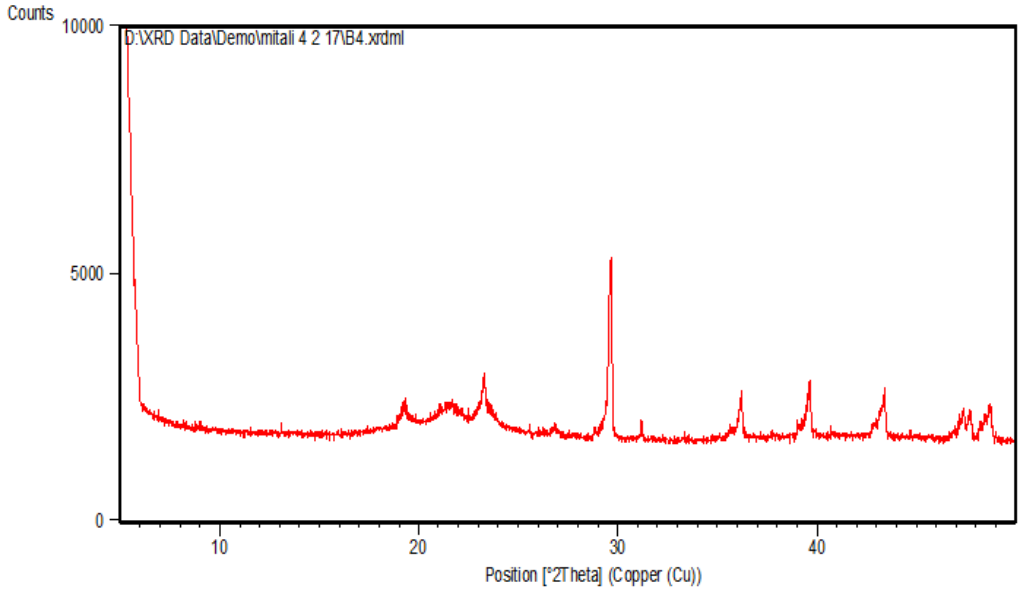

(d)

Figure 6.20: XRD of (a) LH (b) GMS (c) physical mixture of LH and GMS (d) lyophilized LH-SLNs

6.13.8 Transmission Electron Microscopy (TEM)

TEM studies were carried out to get more insights into the morphology of the SLN systems. The TEM image of LH-SLNs show uniform size distribution of lipid nanoparticles (100–150 nm) having dense lipid matrix with spherical shape (Figure 6.21).

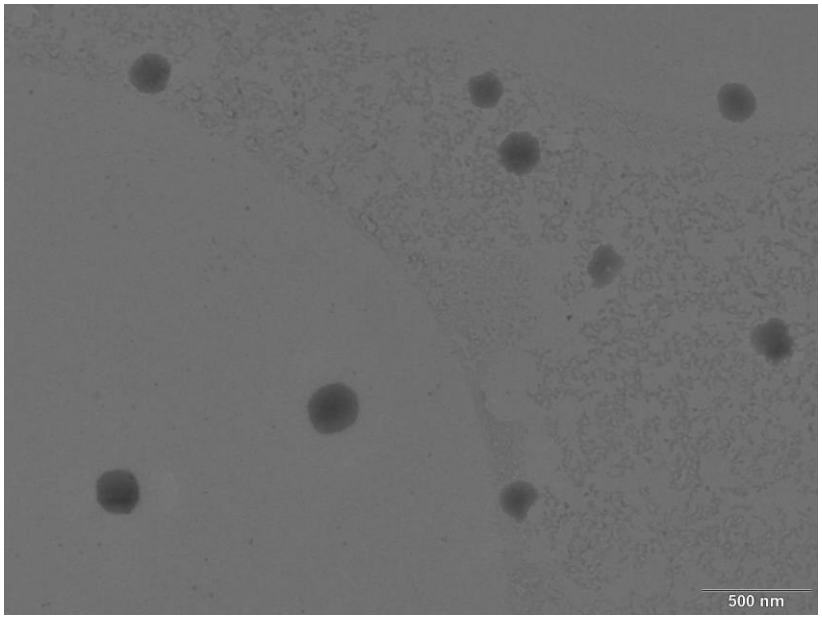

Figure 6.21 : TEM image of optimized batch of LH-SLNs

6.14 IN VITRO DRUG RELEASE STUDY

In vitro drug release profile of LH-SLNs and LH suspension is shown in figure 6.22. The release profile of LH suspension indicated most of the drug (91.44±3.93%) was diffused through dialysis membrane in acidic medium and subsequent release 96.1±2.86% in phosphate buffer.

In contrast, release profile of LH-SLNs showed slow release of drug in acidic medium (<10%) in 2 h. The inclusion of drug into lipid nanoparticles significantly reduced the drug release at gastric pH. After transferring it in phosphate buffer pH 6.8 release medium, it showed slow and controlled drug release (92.09±4.23%) upto 24 h (Figure 6.20). The release profile of LH-SLN exhibited typical biphasic pattern with an initial rapid phase followed by a slow phase. The initial burst release of LH (~32%) can be attributed to rapid release of LH incorporated into the shell followed by a slow, sustained drug release which can be due to the LH entrapped within the core of the SLNs. A possible explanation is a short diffusion path due to an enrichment of drug in the outer region of SLN or drug deposition on the solid surface. Furthermore, the solubility of LH in aqueous phase is increased at high temperatures used to maintain the lipid in molten state which becomes supersaturated at the re-crystallization temperature of the lipid matrix. During re-crystallization the solid lipid core is formed entrapping the drug present in solution. Further lowering of temperature reduces the solubility of LH and the existing lipid core will not allow the drug molecules inside consequently the drug starts crystallizing and gets adsorbed on the surface of the lipid particle (24).

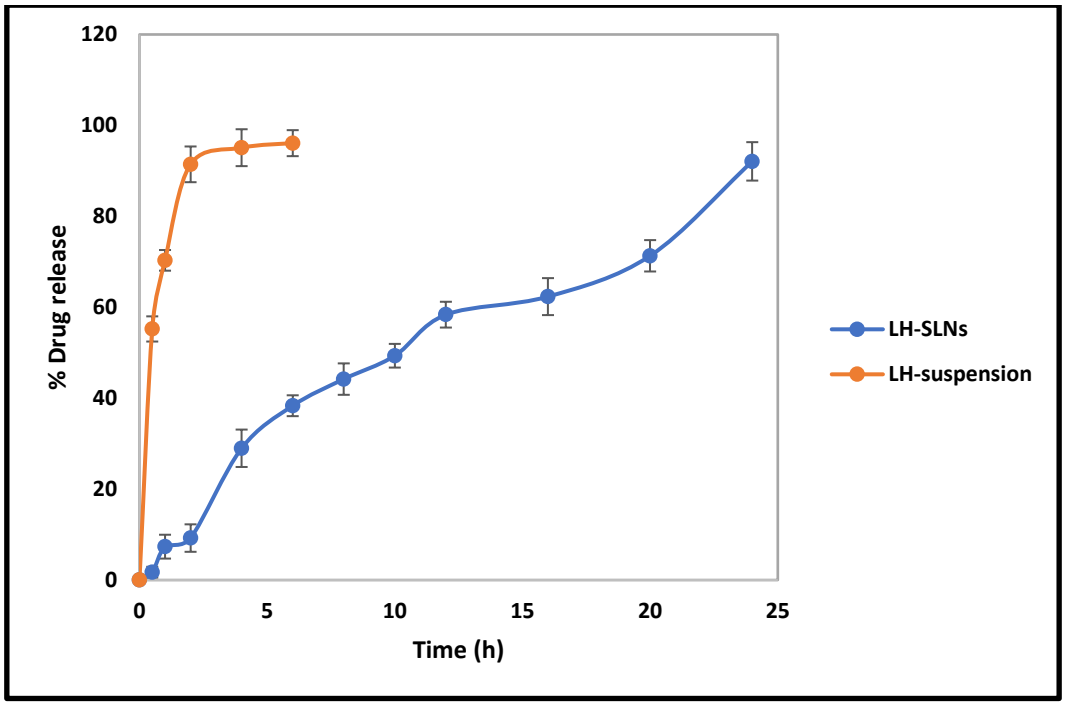

Figure 6.22: In vitro drug release profile of LH-SLNs and drug suspension

Various release models viz. zero order, first order, Korsmeyer–Peppas, Hixson Crowell, Higuchi, Zero-order model and First-order were applied on the release data. Of the various release models, Higuchi release model was best fitted for the developed solid lipid nanoparticles (Table 6.20). Thus, the drug release mechanism was assumed to be controlled by diffusion.

Table 6.20: Correlation coefficient value of LH release kinetics

Formulation code	Correlation coefficient value (R^2)				
	Zero order	First order	Higuchi	Korsmeyer Peppas	Hixon-crowell
LH-SLN	0.9465	0.9136	0.9714	0.8836	0.9508
LH suspension	0.5537	0.8435	0.8224	0.1472	0.7549

The drug release from SLNs is usually considered as a combination of Fickian (diffusion) and non-Fickian transport of drug molecules through the lipid layers (26). Thus, the obtained data were fitted into Korsmeyer–Peppas model to verify the mechanism of diffusion. The value of release exponent (n) is 0.43 for pure Fickian and higher values of n, between 0.43 and 0.85, or n = 0.85, for mass transfer following a non-Fickian mechanism (27,28). When analyzed according to Korsmeyer–Peppas model, the release exponent was found to be 0.543. Therefore, the diffusional release was found to follow anomalous transport (combination of diffusion and erosion

mechanisms). Drug release from the drug suspension was found to be first order kinetics i.e. concentration dependent release.

6.15 EX VIVO PERMEABILITY STUDY

The ex vivo drug permeability profile of LH suspension and LH-SLNs is shown in figure 6.23. In case of LH suspension, 94.30±2.97% of LH was diffused through stomach whereas only 1% LH was diffused through intestine indicating very less amount drug would be reaching to intestine and less amount of drug will be available for lymphatic uptake.

LH loaded SLNs showed only 10.77±1.74% LH was diffused from SLNs in the stomach. Subsequent diffusion of the LH through intestine was relatively slower and total 94.15±4.70% of drug was diffused at the end of 24 h indicating slow and sustained release of LH from LH-SLNs (29). This enhanced permeation might be due to small particle size which provides larger surface area for diffusion and more drug will be available for intestinal uptake. Moreover, small particle size and presence of modulator excipients (Sodium deoxycholate) in the LH-SLNs might lead to an enhanced and effective absorption of LH. Hence, it can be said that permeability of LH was enhanced by incorporating it in SLNs which could help in enhancing oral bioavailability of LH via lymphatic uptake.

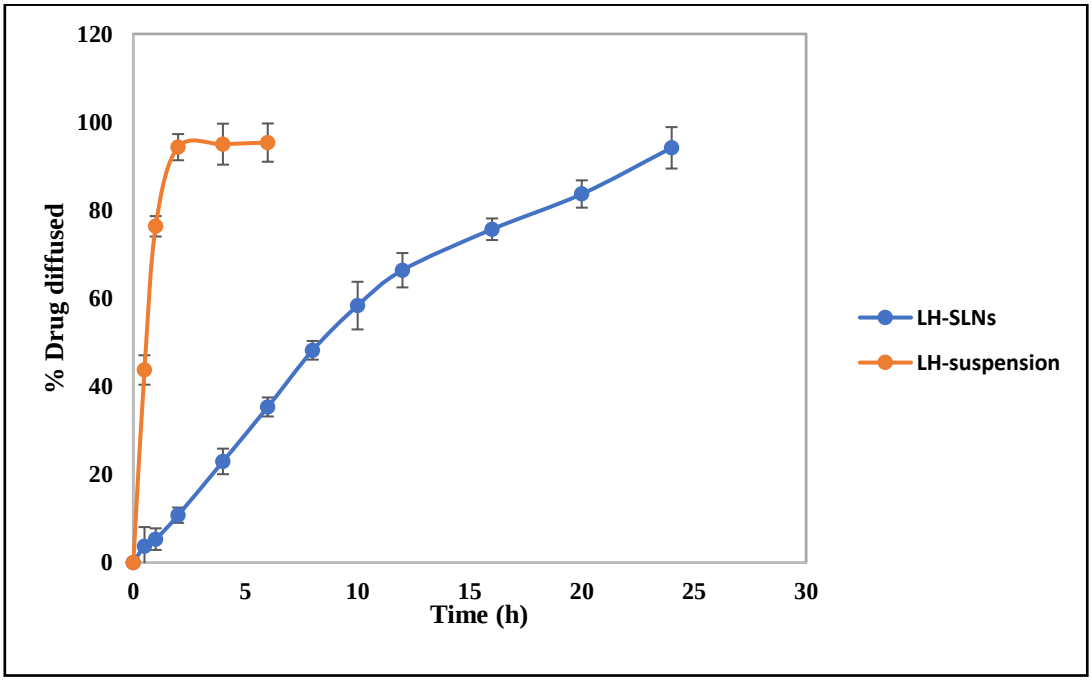

Figure 6.23: Ex vivo drug diffusion profile of LH-SLNs and drug suspension

6.16 STABILITY STUDY

The stability of optimized LH-SLNs was monitored for 3 months at 2-8 °C and RT (30 ± 2°C/60% ± 5% RH) in terms of particle size, zeta potential and drug content (Table 6.21). No significant change was observed in any of the assessed parameters when they were stored at refrigerated condition.

Significant change in all parameters was observed at RT. Drug content was decreased at 30 °C because of drug expulsion from the lipid matrices at higher temperature (30). According to the DLVO theory, a system can be regarded as stable if the electrostatic repulsion dominates the attractive van der Waals forces. The particles have to overcome an energy barrier of electrostatic repulsion to approach closely and form agglomerates. If their velocity or kinetic energy is high enough they will collide. At high temperature (30°C), the kinetic energy of a system increased which dominated the attractive forces (reduced zeta potential) over repulsive forces which may lead to particle aggregation (31). Hence, recommended storage condition for better stability of LH loaded SLN is under refrigeration.

Table 6.21: Characteristics of LH-SLNs after 3-months stability studies at different conditions

Time (months)	**Refrigerated condition (2-8 °C)**			**Room temperature (30±2°C/60% ± 5% RH)**		
	Particle size (nm)	**Zeta potential (mV)**	**Drug content (%)**	**Particle size (nm)**	**Zeta potential (mV)**	**Drug content (%)**
Initial	139.8±3.9	-30.8±3.5	99.2±1.2	139.8±3.9	-30.8±3.5	99.2±1.2
1 month	141.3±4.5	-30.5±2.5	98.7±3.3	154.1±3.3	-28.1±2.1	97.4±3.2
2 months	142.9±3.7	-29.6±3.6	98.1±2.5	178.8±5.3	-26.7±3.7	96.4±2.3
3 months	144.2±2.5	-29.3±2.2	97.3±1.4	213.2±3.9	-22.1±4.5	94.1±4.8

6.17 REFERENCES

1. Lionberger RA, Lee SL, Lee L, Raw A, Yu LX. Quality by Design: Concepts for ANDAs. The AAPS J. 2008;10(2):268-276.
2. International Conference on Harmonization (ICH) (2009) Guidance on industry: Q8 (R2) pharmaceutical development. ICH harmonized tripartite guideline.
3. Patel M, Sawant K. A Quality by Design Concept on Lipid Based Nanoformulation Containing Antipsychotic Drug: Screening Design and Optimization using Response Surface Methodology. J Nanomed Nanotechnol. 2017;8(3):1-11.
4. Park S, Choo G. Hwang S, Kim M. Quality by design: screening of critical variables and formulation optimization of Eudragit E nanoparticles containing dutasteride. Arch Pharm Res. 2013; 36: 593-601.
5. Hao J, Fang X, Yanfang Zhou Y, Wang J, Guo F, Li F, Peng X. Development and optimization of solid lipid nanoparticle formulation for ophthalmic delivery of chloramphenicol using a Box-Behnken design. Int J Nanomedicine. 2011;6:683–692.
6. Qian S, Heng W, Wei Y, Zhang J, Gao Y. Coamorphous Lurasidone Hydrochloride-Saccharin with Charge assisted Hydrogen Bonding Interaction Shows Improved Physical Stability and Enhanced Dissolution with pH-independent Solubility Behavior. Cryst Growth Des. 2015;15(6):2920-2928.
7. Silva AC, Gonzalez-Mirac E, Garciac ML, Egeac MA, Fonsecaa J, Silva J , Santosa D, Soutob EB, Ferreira D. Preparation, characterization and biocompatibility studies on risperidone-loaded solid lipid nanoparticles (SLN): High pressure homogenization versus ultrasound. Colloids Surf B. 2011;86:158–165.
8. Dura n-Lobato M, Enguix-Gonzalez A, Fernandez-Arevalo M, Martin-Banderas L. Statistical analysis of solid lipid nanoparticles produced by high-pressure homogenization: a practical prediction approach. J Nanopart Res. 2013;15:1-14.
9. Xua X, Khan MA, Burgessa DJ. A quality by design (QbD) case study on liposomes containing hydrophilic API: I. Formulation, processing design and risk assessment. Int J Pharm. 2011;419:52– 59.

10. McClements DJ. Edible nanoemulsions: fabrication, properties, and functional performance. Soft Matter. 2011;7:2297–2316.
11. Soares S, Fonte P, Costa A, Andrade J, Seabra V, Ferreira D, Reis S, Sarmento B. Effect of freeze-drying, cryoprotectants and storage conditions on the stability of secondary structure of insulin-loaded solid lipid nanoparticles. Int J Pharm. 2013;456(2) 370-381.
12. Patel PA, Patravale VB. AmbiOnp: Solid Lipid Nanoparticles of Amphotericin B for Oral Administration. J Biomed Nanotechnol. 2011;7:632–639.
13. Floury J, Desrumaux A, Lardieres J. Effect of high-pressure homogenization on droplet size distributions and rheological properties of model oil-in-water emulsions. Innov Food Sci Emerg Technol. 2000;1:127-234.
14. Varia JK, Dodiya SS, Sawant KK. Cyclosporine A Loaded Solid Lipid Nanoparticles: Optimization of Formulation, Process Variable and Characterization. Current Drug Deliv. 2008;5:64-69.
15. Jafaria SM, Assadpoora E, Heb Y, Bhandari B. Re-coalescence of emulsion droplets during high-energy emulsification. Food Hydrocoll. 2008;22:1191–1202.
16. Hakansson A, Fuchs L, Innings F, Revstedt J, Tragardh C, Bergenstahl B. On flow-fields in a high pressure homogenizer and its implication on drop fragmentation. Procedia Food Sci. 2011;1:353 – 1358.
17. https://www.thermofisher.com/order/catalog/product/89904.
18. Xua X, Khan MA, Burgess DJ. A quality by design (QbD) case study on liposomes containing hydrophilic API: II. Screening of critical variables, and establishment of design space at laboratory scale. Int J Pharm. 2012;423:543–553.
19. Bharti Gaba, Mohammad Fazil, Saba Khan, Asgar Ali, Sanjula Baboota, Javed Ali. Nanostructured lipid carrier system for topical delivery of terbinafine hydrochloride. Bulletin Fac Pharm. 2015;53:147–159.
20. Shah MK, Madan P, Lin S. Preparation, in vitro evaluation and statistical optimization of carvedilol-loaded solid lipid nanoparticles for lymphatic absorption via oral administration. Pharm Dev Technol. 2014;19(4):475-485.
21. Mobarak DH, Salah S, and Seham A. Elkheshen SA. Formulation of ciprofloxacin hydrochloride loaded biodegradable nanoparticles: optimization of technique and process variables. Pharm Dev Technol. 2014;19(7):891–900.

22. Khan AA, Mudassir J, Mohtar N, Darwis Y. Advanced drug delivery to the lymphatic system: lipid-based nanoformulations. Int J Nanomedicine. 2013;8:2733–2744.
23. Kuo YC, Chen I. Evaluation of Surface Charge Density and Surface Potential by Electrophoretic Mobility for Solid Lipid Nanoparticles and Human Brain-Microvascular Endothelial Cells. J Phy Chem B. 2007;111:11228-11236.
24. Burra M, Jukanti R, Janga KY, Sunkavalli S, Velpula A, Ampati S, Jayaveera KN. Enhanced intestinal absorption and bioavailability of raloxifene hydrochloride via lyophilized solid lipid nanoparticles. Adv Powder Technol. 2013;24:393–402.
25. Bhandari R, Kaur IP. Pharmacokinetics, tissue distribution and relative bioavailability of isoniazid-solid lipid nanoparticles. Int J Pharm. 2013;441:202– 212.
26. Nabi-Meibodi M, Vatanara A, Najafabadi AR, Rouini MR, Ramezani V, Gilani K, Etemadzadeh SMH, Azadmanesh K. The effective encapsulation of a hydrophobic lipid-insoluble drug in solid lipid nanoparticles using a modified double emulsion solvent evaporation method. Colloids Surf B. 2013;112:408–414.
27. S, Anju SS, Cinu TA, Aleykutty NA, Thomas S, Souto EB. In vivo pharmacokinetics and biodistribution of resveratrol-loaded solid lipid nanoparticles for brain delivery. Int J Pharm. 2014;474:6–13.
28. Costa P, Lobo JMS. Modeling and comparison of dissolution profiles. Eur J Pharm Sci. 2001;13:123–133.
29. Joshi G, Kumar A, Sawant K. Enhanced bioavailability and intestinal uptake of Gemcitabine HCl loaded PLGA nanoparticles after oral delivery. Eur J Pharm Sci. 2014;60:80-89.
30. Ekambaram P, Hasan SAA. Formulation and Evaluation of Solid Lipid Nanoparticles of Ramipril. J Young Pharm. 2011;3(3):216-220.
31. Freitas C, Muller RH. Effect of light and temperature on zeta potential and physical stability in solid lipid nanoparticle (SLN™) dispersions. Int J Pharm. 1998;168:221–229.